TWO-DIMENSIONAL BINDING KINETICS OF INTRACELLULAR ADHESION MOLECULE-1 FOR α_L INSERTED DOMAINS AND β_2 INTEGRINS AT DIFFERENT CONFORMATIONAL STATES

A Thesis
Presented to
The Academic Faculty

By

Fang Zhang

In Partial Fulfillment
Of the Requirements for the Degree
Master of Science in Bioengineering

Georgia Institute of Technology
January 2004

TWO-DIMENSIONAL BINDING KINETICS OF INTERCELLULAR ADHESION MOLECULE-1 FOR α_L INSERTED DOMAINS AND β_2 INTEGRINS AT DIFFERENT CONFORMATIONAL STATES

Approved by:

Dr. Cheng Zhu, Advisor

Dr. Julia E. Babensee

Dr. Periasamy Selvaraj

Date Approved 1/12/04

ACKNOWLEDGEMENTS

I would like to thank my advisor, Dr. Cheng Zhu, for his guidance and help in planning and executing the project. He provided a motivating, enthusiastic, and critical atmosphere during the many discussions we had. I would also like to thank Dr. Timothy A. Springer and Dr. Periasamy Selvaraj for providing critical reagents. I also thank my entire thesis committee, for their time and assistance.

Special thanks to my lab mates who provided help and shared their precious experience thoughout the project and for their friendship. Particullarly, I would like to thank Warren Marcus for providing preliminary data and protocol for this project. I would to express my gratitude to Ning Jiang for leading me through the learning period when I came to the lab and Fang Kong for his assistance in data analysis and blood donation for the experiment.

Last but not least, I would like to thank my parents, for always standing by me and supporting me for all these years.

TABLE OF CONTENTS

LIST OF TABLES

LIST OF FIGURES

LIST OF ABBREVIATIONS

ICAM-1	Intracellular adhesion molecule-1
I domain	Inserted domain
MIDAS	Metal ion dependent adhesion site
RBC	Red blood cell
GPI	Glycosyl phosphatidylinositol
WT	Wild type
k_r	Reverse rate (off-rate)
k_f	Forward rate (on-rate)
K_a	Affinity
P_a	Adhesion probability (frequency)
P_{NS}	Nonspecific adhesion probability
A_c	Contact area
m_l	Site density of ligand
m_r	Site density of receptor
S.E.M.	Standard error of the mean

SUMMARY

Integrins are heterodimeric adhesion molecules consisting of α and β subunits. The β_2 subfamily consists of four members, $\alpha_L\beta_2$, $\alpha_M\beta_2$, $\alpha_X\beta_2$, and $\alpha_D\beta_2$, the first three of which share a common ligand, intracellular adhesion molecule (ICAM)-1. β_2 integrin-ICAM-1 interactions play a major role in inflammatory and other immune responses by regulating leukocyte adhesion and trafficking. To bind ICAM-1, β_2 integrin must convert from inactive to active form, which presumably occurs through conformational change. The activity of β_2 integrin is also regulated by divalent cations. The ligand-binding site of β_2 integrin is located in the inserted (I) domain in the α subunit. Crystallographic studies showed that the I domain exists in two distinct conformations: open and closed.

To examine the effects of the I domain conformations on ligand binding on cell surface, we used micropipette to measure the two-dimensional (2D) kinetics of ICAM-1 reconstituted on red blood cell (RBC) interacting with the isolated α_L I domain on K562 cells, including wild type (WT) and mutant I domains locked in open or closed conformation, as well as their regulation by divalent cations. The results showed an 8000-fold increase in binding affinity of locked open I domain compared to that of the locked closed I domain. As expected, Mg^{2+}, Mn^{2+}, and Ca^{2+} did not affect the binding of the mutant I domains because the conformations were locked. However, after the reduction of disulfide bond with dithiothreitol (DTT), the binding affinity of the open I domain to ICAM-1 was drastically decreased and that of closed I domain to ICAM-1 was increase by 2 folds, suggesting the above binding affinity difference required the presence of the

disulfide bond locking. Moreover, they became regulatable by the divalent cations. The results suggested that the conformational change is the key for binding affinity regulation of I domain on cell surface.

Mg^{2+} and Mn^{2+} were only able to increase the binding affinity of WT α_L I domain by less than 2 folds, indicating their inability to convert the isolated I domain into high affinity conformation. It has been suggested that the activation of I domain requires relay of multiple interdomain conformational changes. To investigate the effects of other domains on the activation of I domain and the propagation of conformational change through the whole integrin, we measured the 2D kinetics of ICAM-1 on RBC to $\alpha_L\beta_2$ on K562 cells and its regulation by divalent cations. Mg^{2+} increased the binding affinity of WT $\alpha_L\beta_2$ ~ 335 folds and to the level comparable to that of the locked open α_L I domain. These data suggested that isolated activated I domain is sufficient for ligand binding but the conformational changes require its interaction with other domains of the integrin.

Physiologically, multiple β_2 integrins are usually expressed on the same leukocyte simultaneously and bind their common ligand concurrently. For this reason, we also determined the 2D kinetics of ICAM-1 for $\alpha_L\beta_2$, $\alpha_M\beta_2$, and $\alpha_X\beta_2$ on neutrophils, which better mimics the physiological situations. The regulation of neutrophil β_2 integrins showed different binding kinetics from K562 cell I domains and $\alpha_L\beta_2$. Mg^{2+} only increased the binding affinity by ~ 42 folds. Our results also indicated that $\alpha_L\beta_2$, $\alpha_M\beta_2$, and $\alpha_X\beta_2$ bind to ICAM-1 independently and $\alpha_L\beta_2$ has the highest binding affinity.

In summary, this is the first application of micropipette technique to measurements of 2D kinetics of the isolated I domains and β_2 integrins. This study

determined the 2D binding kinetics of isolated wild type and mutant I domain, which provided new evidence that the conformational change could regulate the ligand-binding affinity of I domain when it is bound to cell surface. Their regulation by divalent cations showed that different mechanisms of effects of divalent cations on I domain. The 2D binding kinetics of whole β_2 integrins at different conformational states induced by divalent cation not only confirmed the binding potent of isolated activated I domain also revealed the role of other domains in I domain affinity regulation. The initial measurements of neutrophil β_2 integrin kinetics showed that their concurrent ICAM-1 binding is independent and the relative contributions of the three β_2 integrins. These results would add 2D kinetics data to our current knowledge and most importantly provide insights into the conformational change and function of I domain and β_2 integrins.

CHAPTER I

OBJECTIVES

Receptor-mediated cell adhesion plays important roles in many cellular processes, including proliferation, differentiation, and migration. Integrins are a major family of cell surface receptors that mediate cell-cell and cell-matrix interactions. $\alpha_L\beta_2$, $\alpha_M\beta_2$, and $\alpha_X\beta_2$ are members of the β_2 integrins that are exclusively expressed on leukocytes and share a common ligand, intercellular adhesion molecule (ICAM)-1. Conformational changes in the integrins, including that in the ligand-binding site containing inserted (I) domain, is a key mechanism for affinity regulation in integrins.

The following aims were proposed to investigate the relationship between the conformation and the binding function of isolated I domain and whole β2 integrin as well as the regulation by divalent cations.

1. Measure the two-dimensional binding kinetics of ICAM-1 for the wild type and mutant isolated α_L I domains on K562 cells and their divalent cation regulation.

The structural studies of I domains have revealed the existence of two conformations termed open and closed respectively. Mutant α_L I domains locked in either the open or the closed conformation have been generated (Lu *et al.,* 2001). Three-dimensional (3D) binding kinetics measurements revealed that the open I domain has a much higher affinity for ligand than the closed I domain (Shimaoka *et al.,* 2001). However, the two-dimensional (2D) binding kinetics of the cell surface bound I domains were lacking. Using micropipette adhesion frequency assay, we measured the binding

kinetics of the mutant isolated α_L I domains as well as the wild type I domain for ICAM-1. The results provided insights into the effects of the conformational changes on the binding affinity of the I domain on cell membrane.

Divalent cations are major regulators of integrin binding affinity by inducing conformational changes or stabilizing conformers. We measured the 2D binding kinetics of wild type (WT) and mutant I domains in the presence and absence of divalent cations with or without dithiothreitol (DTT) treatment to release the locked conformation. The experiment with or without DTT further confirmed that the dramatic difference in binding affinities of the open and closed I domain was induced by the difference of conformations that locked by the disulfide bonds. The divalent cation studies not only quantified the effects of divalent cation on isolated I domains, also provided evidence for the inability of isolated I domain to change the conformation by itself.

2. Measure the 2D binding kinetics of ICAM-1 for $\alpha_L\beta_2$ on K562 cells and their divalent cations regulation.

Although the I domain is where the ligand binding site resides, other domains play important roles in conformational changes of the whole integrin and in the conformation regulation of the I domain. Shimaoka *et al.* (2002) proposed that the I domain is activated by allosteric interactions with the I-like domain. By measuring the binding kinetics of inactive/active intact $\alpha_L\beta_2$ on K562 cells, we elucidated the effects of other domains on I domain conformational changes. Moreover, the binding kinetics of isolated I domain and intact integrin were compared to demonstrate the adhesion efficiency of the isolated I domain.

Besides the metal ion-dependent adhesion site (MIDAS) in the I domain, there are several additional divalent cation coordination sites in the whole integrin. However, their significance is not clear (Hynes, 2002) and the precise mechanisms of the activation/inactivation by divalent cations are unknown. Here, we examine the effects of Mg^{2+}, Mn^{2+} and Ca^{2+} on the whole $\alpha_L\beta_2$. These studies could help to address the physiological relevance of the conformations locked by disulfide bonds. The importance of other domains in integrin was also investigated by comparing the difference of activation by Mg^{2+} between the WT isolated α_L I domain and the WT $\alpha_L\beta_2$.

3. Determine the 2D kinetics of ICAM-1 for neutrophil β_2 integrins at different conformational states and whether the binding of $\alpha_L\beta_2$, $\alpha_M\beta_2$, and $\alpha_X\beta_2$ to ICAM-1 is independent or cooperative.

Three of the neutrophil β_2 integrins, $\alpha_L\beta_2$, $\alpha_M\beta_2$, and $\alpha_X\beta_2$, bind to ICAM-1. Due to the critical role of neutrophil β_2 integrins in immune responses, extensive research has been conducted to investigate their function and regulation *in vivo* and *in vitro*, most of which were population studies (Neelamegham *et al.*, 1998; Von-Andriam *et al.*, 1995; Abitorabi *et al.*, 1997). However, the quantitative 2D kinetic data for the binding between ICAM-1 and β_2 integrins on single cells were not available. We measure the 2D binding kinetic constants of ICMA-1 on red blood cell (RBC) for $\alpha_L\beta_2$, $\alpha_M\beta_2$, and $\alpha_X\beta_2$ on neutrophil when they are at different conformational states induced by divalent cations, which not only adds lacking kinetic data to present knowledge but provides comparison for the isolated I domain and $\alpha_L\beta_2$ on K562 cells.

$\alpha_L\beta_2$, $\alpha_M\beta_2$, and $\alpha_X\beta_2$ bind concurrently when a neutrophil is in contact with an

ICAM-1 expressing cell. It is not clear whether the three integrins cooperate with each other or not. However, there is evidence showing that they independently bind to ICAM-1 (Ding *et al.,* 1999). Here, we measure the binding kinetics of ICAM-1 for individual β_2 integrin on neutrophil and fit the data to an independent concurrent binding model to test the hypothesis of independent binding.

CHAPTER II

BACKGROUND

Cell Adhesion Molecules and β_2 Integrins

Cell adhesion is mediated by specific molecular interactions of proteins or carbohydrates referred to as receptors and ligands, or cell adhesion molecules. The known families of cell adhesion molecules include integrins, cadherins, selectins, and members of the immunoglobin (Ig) superfamily. The receptors mediate adhesion by binding their counter-receptors, or ligands, which are located either on neighboring cells or in the extracellular matrix. Receptor-mediated cell adhesions usually involve concurrent binding of multiple species of receptors and ligands and take place as a dynamic process.

Integrins are a family of cell surface receptors that integrate the cytoskeleton with points of attachment in the extracellular environment to mediate cell adhesion, polarization, and migration. Integrins are heterodimeric transmembrane molecules composed of a α subunit (~120–180 KDa) and a β subunit (~90–120 KDa). So far, at least 18 different α subunits and 8 β subunits have been described in vertebrates (Humphries *et al.*, 2000), forming at least 24 heterodimers (Figure 2-1).

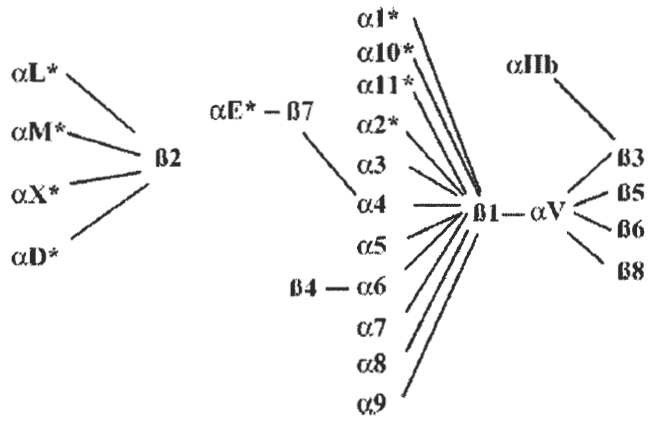

Figure 2-1. The integrin family of adhesion receptors (Shimaoka *et al.,* 2002). Lines denote the αβ pairings. Those integrins contain the I domain are indicated (asterisks).

The β_2 integrin subfamily includes four members, which compose of four different α subunits α_L, α_M, α_X, and α_D (CD11a, b, c and d) noncovalently associated with a common β_2 (CD18) subunit (Figure 2-1). The expression of β_2 integrins is restricted to leukocytes. $\alpha_L\beta_2$ (lymphocyte function-associated antigen-1 or LFA-1) is present on nearly all leukocytes. It mediates leukocyte adhesion to cells bearing any of the three counter-receptors, ICAM-1, -2, and -3 (Springer, 1995). $\alpha_M\beta_2$ (complement receptor 3 or CR3, Mac-1) and $\alpha_X\beta_2$ (CR4, p150,95) are found on monocytes, macrophages, granulocytes, large granular lymphocytes, and a subpopulation of immature B cells. $\alpha_M\beta_2$ binds to ICAM-1, iC3b, fibrinogen, and serum factor X, and other substances. $\alpha_X\beta_2$ binds to iC3b, fibrinogen, and ICAM-1 (Blackford *et al.,* 1996). $\alpha_D\beta_2$ preferentially binds to ICAM-3 (Danilenko *et al.,* 1995). Cell-cell adhesions mediated by these integrins contribute to many physiological processes of leukocytes,

such as antigen presentation, cytotoxicity and phagocytose. They also cooperate with the selectin adhesion receptors to guide T cells into lymphatic areas and in other tissues. They direct leukocyte migration across endothelia in inflammatory reaction in response to insult and injury. The discovery of the genetic basis of an inherited disease called leukocyte adhesion deficiency (LAD) syndrome, which manifests as defect in leukocyte adhesion and is caused by the lack of expression of β_2 integrins on the cell surface, underscored the important biological role of these receptors in the inflammatory and immune responses (Crowley *et al.,* 1980).

β_2 Integrin Domain Structure Organization

β_2 integrins are transmembrane molecules. Each of their two subunits spans the plasma membrane once and has a short cytoplasmic tail. The N-terminal half of the α subunit's extracellular portion contains seven tandem repeats, which are predicted to adopt a β-propeller fold. In all four β_2 integrins as well as $\alpha_1\beta_1$, $\alpha_2\beta_1$, $\alpha_{10}\beta_1$, $\alpha_{11}\beta_1$, and $\alpha_E\beta_7$ integrins, an additional highly conserved inserted (I) domain (or A domain, also designed as α–I/A domain), approximately 200 amino acids long, is found between the second and third repeats of the β-propeller domain (Springer, 1997). The C-terminal half of the α subunit's extracellular portion is the stalk region. There are three β-sandwich domains in this region, including the thigh, Calf-1, and Calf-2 domains (Figure 2-2). The N-terminal region of β_2 subunit contains a PSI (Plexin, Seaphorins, and Integrin) domain. It also contains an evolutionarily conserved domain termed I-like domain (or βA

domain). This domain appears to directly bind ligand in integrins that lack I domain and to indirectly regulate ligand binding of the I domain in I domain- containing integrins. The hybrid domain is folded from amino acid sequence segments on either side of the I-like domain. The C-terminal half of the extracellular portion of the β subunit contains four cysteine-rich repeats, called integrin-epidermal growth factor (I-EGF) 1-4 domains, which are characteristic of all integrin β subunits (Goodman & Bajt, 1996), and a β-tail (βT) domain (Figure 2-2).

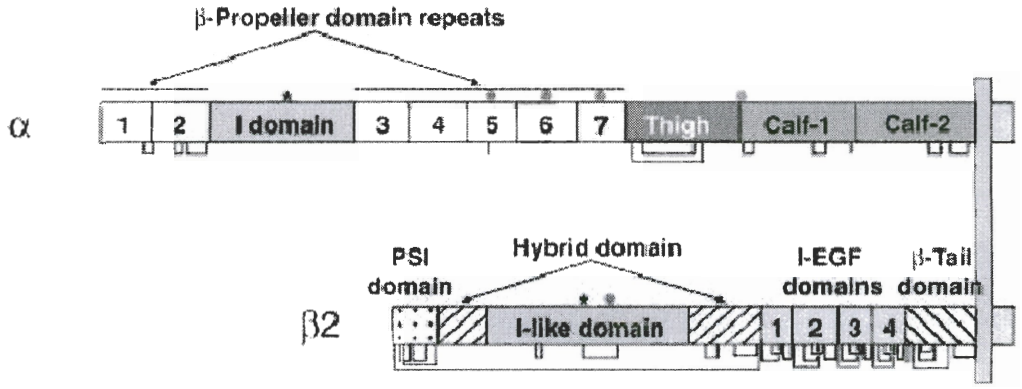

Figure 2-2. The domain arrangement of the primary structure of β_2 integrins (Shimaoka *et al.*, 2002).

Structure and Conformational Changes of the Inserted Domain

I domain is the major ligand binding site for I domain-containing integrins. Recombinant I domain binds ligand with the same specificity as the parental integrin and the binding is also in a same cation-dependent manner (Dickeson & Santoro, 1998). The deletion of the I domain abolished ligand binding in the context of the intact integrin (Leitinger & Hogg, 2000).

The α_M I domain is the first crystallized domain of integrin (Lee *et al.,* 1995). Since then, three more crystal and nuclear magnetic resonance (NMR) structures have been determined for I domains from the integrin α_L (Qu & Leathy, 1995; Qu & Leathy 1996; Legge *et al.,* 2000; Kallen *et al.,* 1999), α_2 (Emsley *et al.,* 1997; Emsley *et al.,* 2000), and α_1 (Nolte *et al.,* 1999) subunit. These studies have provided critical new insights into I domain structure and function.

I domain assumes a dinucleotide-binding fold with α-helices surrounding a central β-sheet a with a metal ion coordinating site on one end (defined as the top of the domain) and is connected through the adjacent N and C termini on the opposite end (bottom) to the body of the integrin (Figure 2-3). The metal-coordinating residues and the residues surrounding the metal-binding site form the binding site for several physiologic ligands. Therefore, this site has been designated as the metal ion-dependent adhesion site (Lee *et al.,* 1995b).

The integrin WT α_M (Lee *et al.,* 1995), α_2 (Emsley *et al.,* 2000) and α_L (Qu & Leahy 1995, 1996; Kallen *et al.,* 1999; Legge *et al.,* 2000) as well as mutant α_L I domains (Shimaoka *et al.,* 2003) were found to crystallize in two different conformations, which were termed open and closed conformers. In the open structure, an acidic residue donated either by a ligand or by a ligand mimetic lattice contact contributes to the metal ion coordination sphere in the MIDAS. The metal ion is central to the binding site and directly coordinates a Glu residue in the ligand (Figure 2-4) (Shimaoka *et al.*, 2001). By comparison, no ligand-like contact in the closed structures has been determined (Figure 2-4). The structural rearrangement of the MIDAS is coupled to backbone movements of

the loops that bear the coordinating residues. The open and closed conformations also differ in the position of the C-terminal α7 helix (Figure 2-5). The transition from the closed to the open structure is linked to a large 10 Å downward movement of the C-terminal α7 helix and a repacking of the hydrophobic face of the α helix (Tagaki & Springer, 2002).

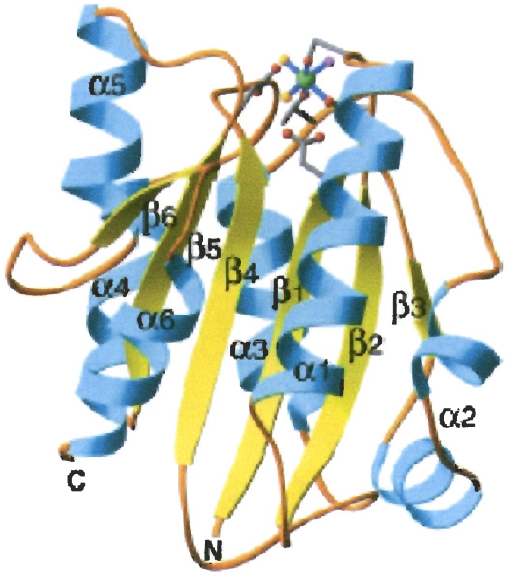

Figure 2-3. Ribbon diagram of the α_M I domain (Shimaoka *et al.,* 2002). The β-strands (yellow), α-helices (cyan), and the N and C termini are labeled. The Mg ion coordinated in MIDAS is shown as a green sphere.

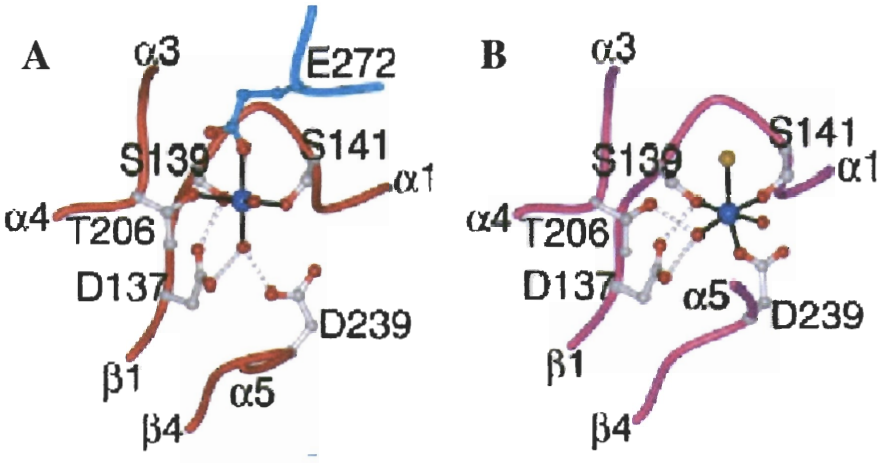

Figure 2-4. MIDAS structures of (A) the pseudo-liganded high-affinity I domain, (B) the unliganded WT I domain (Shimaoka *et al.*, 2003). The ligand mimetic molecule is colored cyan. The metal ions are colored blue, water molecule and ligating side chain oxygen atoms are colored red, and the chloride ion from the wild-type I domain structure is colored orange. The MIDAS residues and Glu-272 from a lattice mate I domain in (A) are shown as ball-and-stick models. Metal coordination and hydrogen bonds are represented by solid black lines and gray dotted lines, respectively.

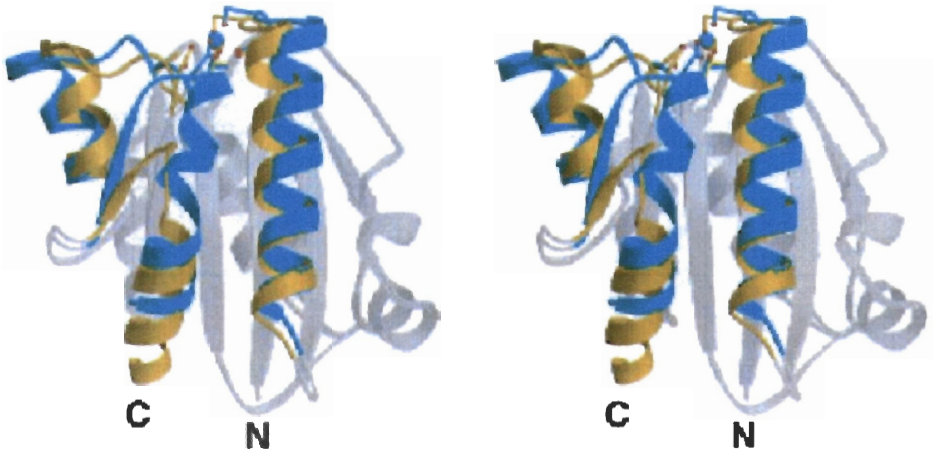

Figure 2-5. Stereo view of the alternative conformations of α_M I domain (Tagaki *et al.*, 2002). The regions of significant difference between the superimposed conformers are shown in yellow (open) and cyan (closed). Similar backbone regions are in gray. Metal atoms and coordinating sidechain bonds and carbon atoms are in yellow (open) and blue (closed); oxygen atoms are red.

There was considerable controversy about whether the different conformations were physiologically relevant or were an crystallographic artifact (Baldwin *et al.*, 1998; Liddington & Bankston., 1998). To resolve this issue, it is very critical to know whether the conformational changes seen in crystal structures alter affinity for ligand as predicted, whether the change in affinity is substantial, and whether conformational changes in I domains occur on cell surface in physiological circumstances (Takagi & Springer, 2002).

Recent studies provided evidence that the open and closed conformers correspond to the high and low affinity states. The finding that one I domain, α_2, crystallized in the closed form in the absence of ligand, but in the open form in its presence, suggested that the ligand may trigger or stabilize the high affinity state (Emsley *et al.*, 2000). Xiong *et al.* (2000) described the binding isotherms and structure of stable and homogeneous low and high affinity forms of the α_M I domain. The high affinity form generated by mutation crystallized in the open conformation and induced a high affinity state when introduced in the $\alpha_M\beta_2$ receptor. Kallen *et al.* (1999) reported that lovastatin, a drug that stabilize the closed conformation, inhibited the interaction of human LFA-1 with its counter-receptor ICAM-1. Furthermore, mutations have been introduced to stabilize a particular conformation, and tested for effect on ligand binding. Both the open and closed conformations of the α_M I domain were stabilized with different mutations to investigate the physiological significance of these conformations. Designed open I domains showed increased binding to ligand when expressed on the cell surface in $\alpha_M\beta_2$ heterodimers, whereas designed closed or wild type I domains did not (Shimaoka *et al.*, 2000).

Similar studies were also carried out to lock α_L I domain in either open or closed

conformation using the structure of the open α_M I domain as a template (Lu *et al.,* 2001). The candidate positions were chosen far away from the MIDAS and thus presumed not to disturb the structure and function of the binding site. The positions were found bracket the loop between the C-terminal α-helix and the preceding β-strand (Figure 2-6 A). A pair of cysteines was introduced to lock this loop in two alternate conformations. The mutations were at residues 287 and 294 for the open conformation, and at residue 289 and 294 for the closed conformation (Figure 2-6 B).

The mutants were tested for ligand binding to investigate the effect of conformational change. In SPR measurements of binding to ICAM-1, the soluble locked open α_L I domain showed a 9000-fold increase in affinity compared to wild type and locked closed conformers; the affinity of locked closed I domain was similar to that of the wild type (Shimaoka *et al.,* 2001). Furthermore, the affinity and kinetics of the soluble locked open I domain for ICAM-1 were comparable to those measured independently in SPR (Labadia *et al.,* 1998) for intact, activated $\alpha_L\beta_2$. These results demonstrated that the open and closed conformations correspond to high and low affinity ligand binding conformations, respectively. They also suggested that the conformation and position of the C-terminal α helix and the preceding loop is fully sufficient for regulating the affinity of ligand binding at the MIDAS.

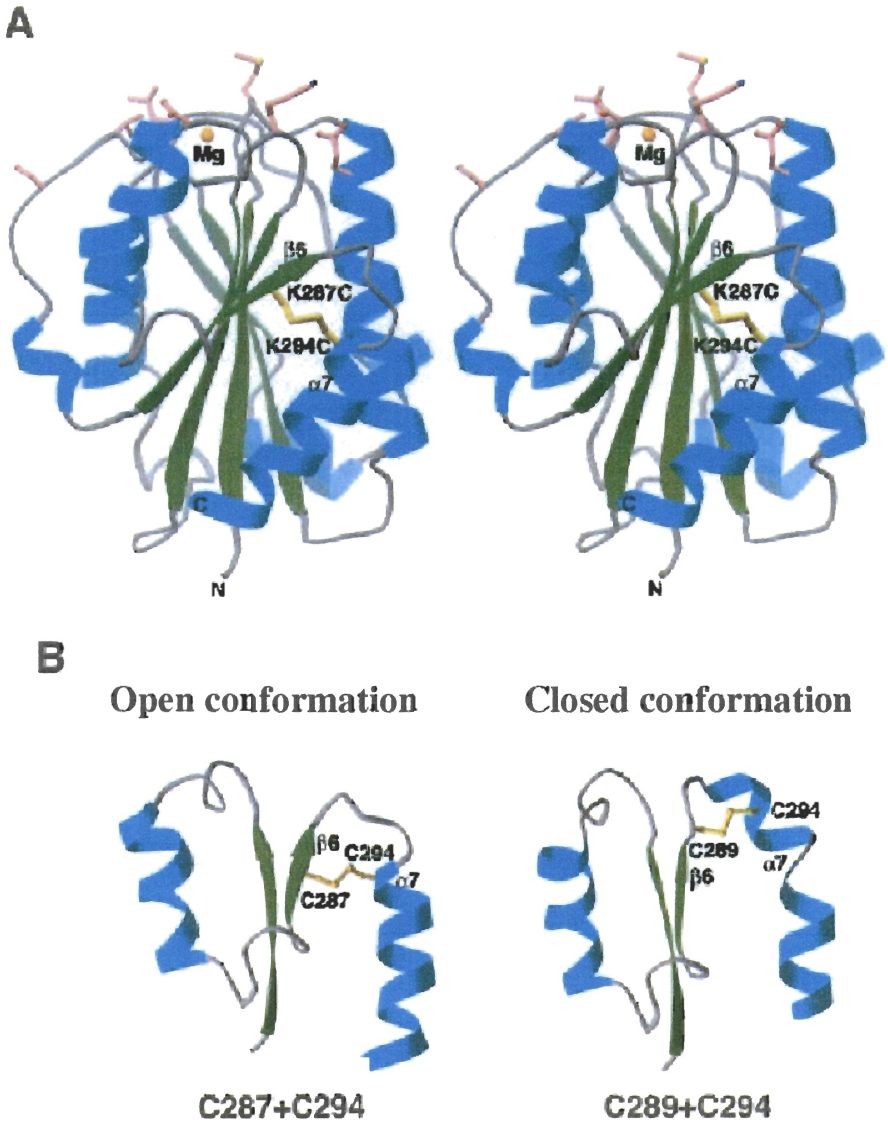

Figure 2-6. Mutant α_L I domains (Shimaoka *et al.*, 2001). (A) Stereodiagram of the open conformation model of the α_L I domain, with mutations to introduce a disulfide bond. The side chains and disulfide bond of C287 and C294 are shown in yellow. The Mg^{2+} ion of the MIDAS is shown as a gold sphere. Sidechains of residues important in binding to ICAM-1 are shown with rose-pink sidechains and yellow sulfur, red oxygen, and blue nitrogen atoms. Note that these residues surround the Mg^{2+} ion and are distant from the disulfide. (B) Predicted disulfide bonds that are selective for open (left) or closed (right) conformers of the αL I domain. Only residues 254–305 of the models are shown. The downward movement of the α7 helix in the left panel compared to the right panel is readily apparent.

Table 2-1. The kinetic rates and dissociation constants for ICAM-1 to the WT, open and closed α_L I domains and the intact $\alpha_L\beta_2$.

Immo. Ligand	Analyte	k_f ($M^{-1}s^{-1}$)	k_r (s^{-1})	K_d (μM)
sICAM-1	WT I domain	2950±400	4.95±0.85	1670±100
sICAM-1	closed I domain	2110±400	2.84±0.27	1760±70
sICAM-1	open I domain	139000±8000	0.0257±0.0015	0.185±0.012
open I domain	sICAM-1	107000±3000	0.0275±0.0028	0.258±0.024
$\alpha_L\beta_2$	sICAM-1	224000±69000	0.0298±0.0069	0.133±0.041

Binding kinetics measured by SPR. Data are from Shimaoka *et al.* (2001), except for that of $\alpha_L\beta_2$, which were from Labadia *et al.* (1998)

Since the structure of I domain in the context of the integrin heterodimer is not known yet, the details of the interdomain movement that convert the I domain into the open conformation are not understood. The high affinity ligand binding of locked open I domain was induced by the engineered disulfide bonds that pulled the α7 helix or linker downward (Shimaoka *et al.,* 2003; Lu *et al.,* 2001; Shimaoka *et al.,* 2001; Shimaoka *et al.,* 2002). Cell rolling assay suggested that the wild type I domain was able to support rolling of cells in shear flow, where force exerted on the C-terminus of the I domain helped to stabilize it in the high affinity conformation (Salas *et al.,* 2002). This finding support a present most probable model for I domain activation, i.e., a downward movement of the C-terminal α helix induced by the exertion of a bell-rope-like pull by other domains, such as I-like domain in the β subunit (Takagi & Springer, 2002).

The results with soluble α_L I domains provided insight into the effects of

conformational change on binding affinity; however, they should be complemented by studying on how the wild type and mutant α_L I domains behave when they are bound to cell membrane. It is important to measure the 2D kinetics of I domain ligand binding for a complete understanding since integrins are cell surface molecule instead of soluble molecules.

Structure and Conformational Changes of the Extracellular Portion of Integrins

Unlike selectins, β_2 integrins do not constitutively recognize ligand but require cellular activation to form stable bonds with endothelial ligands (Lum *et al.,* 2002). The ability of their extracellular domains to bind ligands can be dramatically increased on a timescale of less than 1 second by signals within the cell (Shimaoka *et al.,* 2002). This feature is very important for normal functions of platelets and leukocytes in thrombotic and inflammatory processes. Inactivated or resting state of the integrins allows platelets and leukocytes to circulate in the blood stream without binding to normal blood vessel wall. Activation of integrins on these cells enables platelets to bind to injured vessel walls and fibrin clots immediately, and enables leukocytes to bind to vessel walls and subsequently to migrate across the endothelium.

It has been suggested that the activation of integrins on cell surface is accomplished by conformational changes of the extracellular domains. Electronic microscopy studies showed that the extracellular portion of integrins contain a globular headpiece, and two long stalk regions containing C-terminal segments from the α and β subunits connecting the headpiece to the transmembrane and the cytoplasmic domains

(Du *et al.*, 1993; Takagi *et al.*, 2001). In 2001, the first X ray crystal structure of the extracellular domain of an integrin was published (Xiong *et al.*, 2001). It was a big surprise that the crystal structure of the extracellular fragment of integrin $\alpha_V\beta_3$ assumed a bent conformation, in which the ligand-binding headpiece is folded back onto the tailpiece of the molecule (Figure 2-7 A). It has been proposed, but not shown, that β_2 integrin also adopts the bent V-shape conformation. The position of the I domain shown in Figure 2-8 is only a model because no integrin that contains an I domain has been crystallized yet.

It is not clear whether the bent conformation is an artifact due to the crystal lattice contact or not. Takagi *et al.* (2002) observed two conformations of $\alpha_V\beta_3$ in electron microscopy (EM) study. In the presence of Ca^{2+}, the integrin shows a compact V-shape appearance with a size and shape closely matching the reported crystal structure (Figure 2-7A), which indicated that the bent integrin conformation is physiological. They also showed that this bent conformation has low affinity for biological ligands. Addition of Mn^{2+} resulted in a switchblade-like opening to an extended structure that fits the standing $\alpha_V\beta_3$ integrin modeled based on the crystal structure (Figure 2-7B), which is accompanied by a dramatic increase in affinity for its physiologic ligand. The results suggested that Mn^{2+} induces breakage of the large interface between the headpiece and tailpiece in the bent conformation, and the straightening of the bent at the genu. Therefore, integrins on resting cell surface may essentially assume in the bent conformation and that a conformational rearrangement is required for integrin activation (Takagi & Springer, 2002).

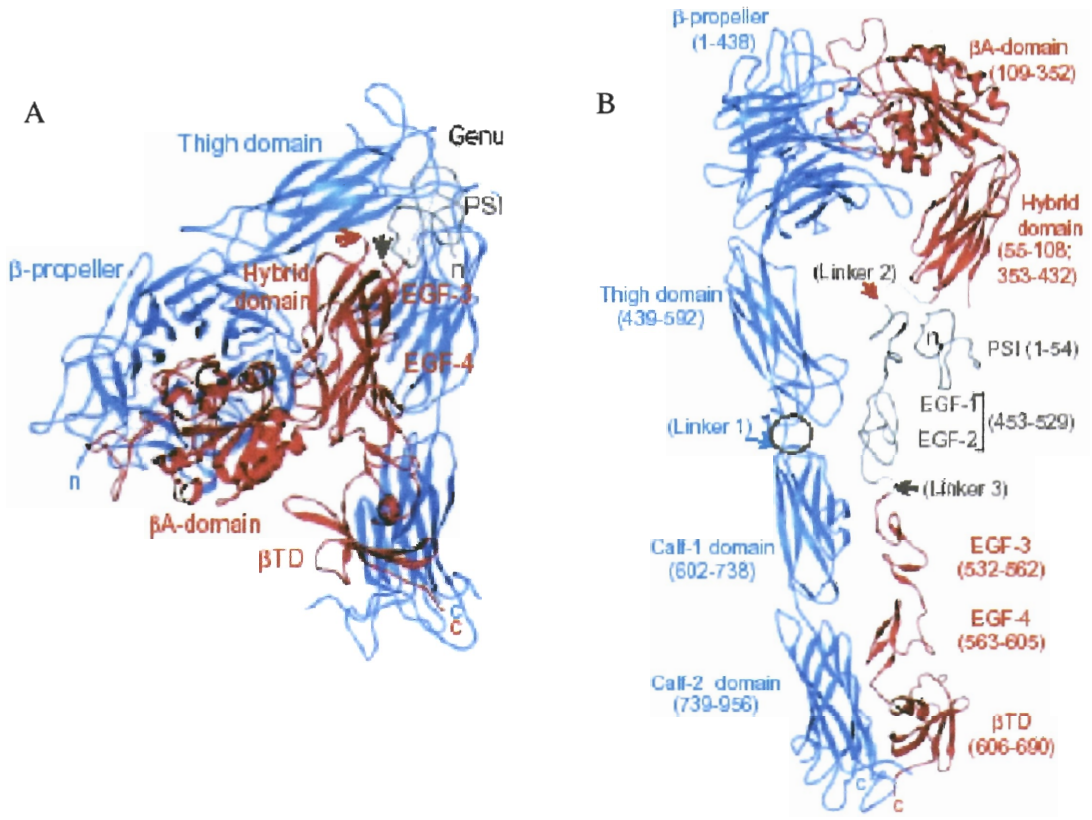

Figure 2-7. Structure of the extracellular segment of $\alpha_V\beta_3$ (Xiong *et al.*, 2001). (A) Ribbon diagram of crystallized $\alpha_V\beta_3$ [shown in blue (α_V) and red (β_3)]. (B) Model of the extended extracellular segment of $\alpha_V\beta_3$.

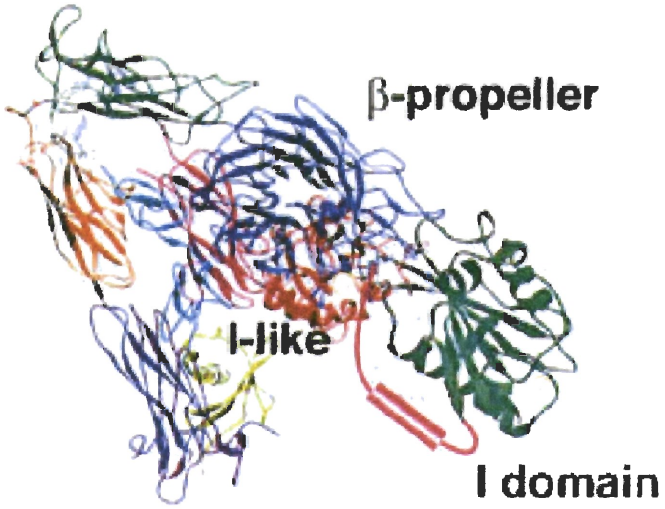

Figure 2-8. Model for extracellular segment of $\alpha_L\beta_2$ at resting state (Shimaoka *et al.,* in press). The model for all the extracellular domains except for the I domain are based on conformational states of $\alpha_V\beta_3$ and $\alpha_L\beta_2$ defined by negatively stained electron microscopy (Tagaki *et al.*, 2002), crystallography (Xiong *et al.*, 2002), NMR (Beglova *et al.*, 2002). The α_L I domain is a cartoon based on crystal structures (Shimaoka *et al.*, 2003).

Recently, the accumulated structural and functional data provide strong support for the following integrin conformational regulation model (Takagi *et al.,* 2002). The cytoplasmic domain regulates the integrin activation by initiating the separation of the α and β subunit cytoplasmic and transmembrane domains. As a consequence, the extracellular interface between the two subunits in the tailpiece becomes destabilized, which facilitates the switchblade-like opening. The disruption of this interface enables the hybrid domain to swing out from the I-like domain in the β subunit, facilitating the downward movement of the I-like domain C-terminal α helix that is coupled to I-like domain MIDAS rearrangement (Figure 2-10). For the I domain containing integrins, an "intrinsic ligand" α subunit residue has been proposed to bind to the activated I-like

domain MIDAS. This binding pulls the C-terminal α helix of the I domain downward and converts it to the activated conformer for high affinity ligand binding (Alonso *et al.*, 2002; Shimaoka *et al.,* 2002) (Figure 2-10).

Both EM studies (Takagi *et al.,* 2002) and kinetic measurements of I domains (Shimaoka *et al.,* 2001) indicated that multiple conformational states of integrin coexist. It has been suggested that the regulation of integrin conformation should be viewed as a shifting of the dynamic equilibrium among three conformers, a bent conformation, an extended conformation with a closed headpiece, and an extended conformation with an open headpiece, rather than the flipping of a switch (Shimaoka *et al.,* in press; Carman & Springer, in press; Luo *et al.,* 2003) (Figure 2-9).

Although rapid progress has been made in the past decade for understanding structure and function of integrins, there are a lot of puzzles waiting for resolving. For example, regarding for the above model, it is not known whether the same conformational changes observed for I domain also take place in the I-like domain as proposed. Most importantly, there was no direct evidence for the very complicated long-range conformational propagation. For I domain containing integrins, the key step of activation would be the conversion of I domain MIDAS into high affinity. It is essential to understand the role of other domains in regulation of I domain.

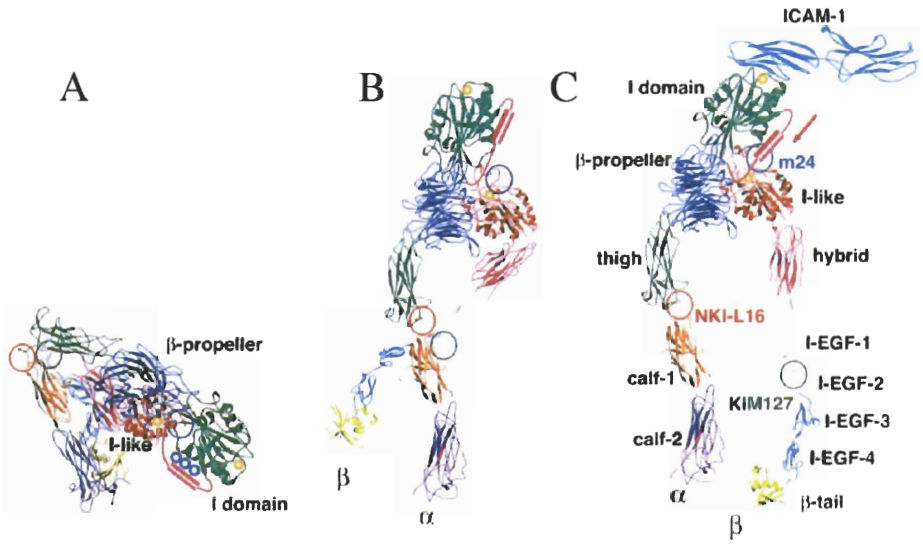

Figure 2-9. Model for global conformational states of the extracellular domain of $\alpha_L\beta_2$ (Shimaoka *et al.*, in press). (A) Bent conformation. (B) Extended conformation with closed headpiece. (C) Extended conformation with open headpiece.

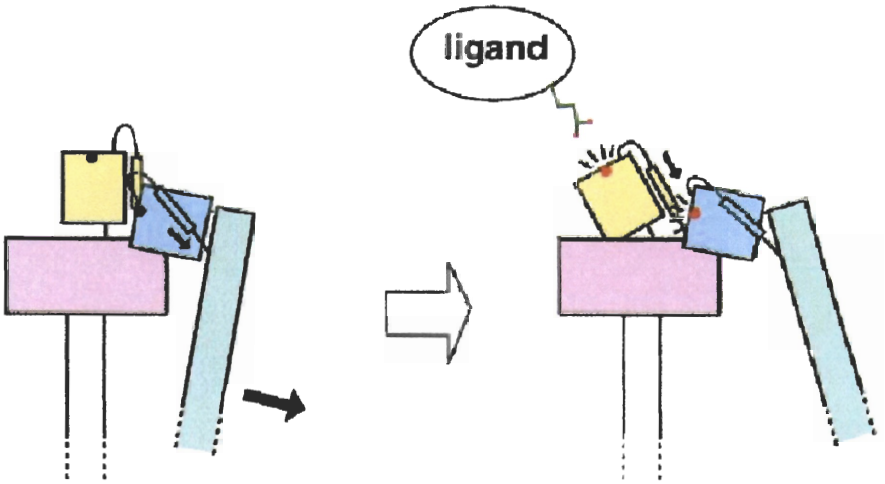

Figure 2-10. Model of conformational changes of I-domain containing integrins that result in activation (Takagi & Springer, 2002). Swinging away the hybrid domain (light green) pulls the C-terminal α-helix of the I-like domain (light blue), converting the low-affinity MIDAS (black dot) to the high affinity MIDAS (red dot). The activated I-like domain MIDAS in turn ligates and pulls the C-terminal α-helix of the I domain (yellow), converting the I domain MIDAS to the high-affinity conformation that is ready for interaction with ligand.

Intracellular Adhesion Molecule-1

ICAM-1 (CD54) is a type I transmembrane glycoprotein of 85–110 KDa composed of five immunoglobin superfamily (IgSF) domains, a transmembrane domain, and a short cytoplasmic tail that binds α-actin (Figure 2-11A) (Dustin *et al.,* 1986; Carpén *et al.,* 1992). It is important for granulocyte extravasation, lymphocyte mediated cytotoxicity, and the development of specific Immunological responses involving cell-cell interactions (Jun *et al.* 2001). Among the five Ig-like domains (D1-5) of ICAM-1, only the structure of domains 1-2 has been solved in X-ray crystallography (Figure 2-11B). The single most important residue for binding is Glu-34, which has been shown to ligate the Mg^{2+} in the MIDAS of the I domain (Shimaoka *et al.,* 2003) (Figure 2-11B). Although there are differences between ICAM-1s in different species, Johnston *et al.* (1990) showed that human $\alpha_L\beta_2$ also specifically bind to mouse ICAM-1 and the cross-species binding is unidirectional, that is, mouse $\alpha_L\beta_2$ could not bind to human ICAM-1.

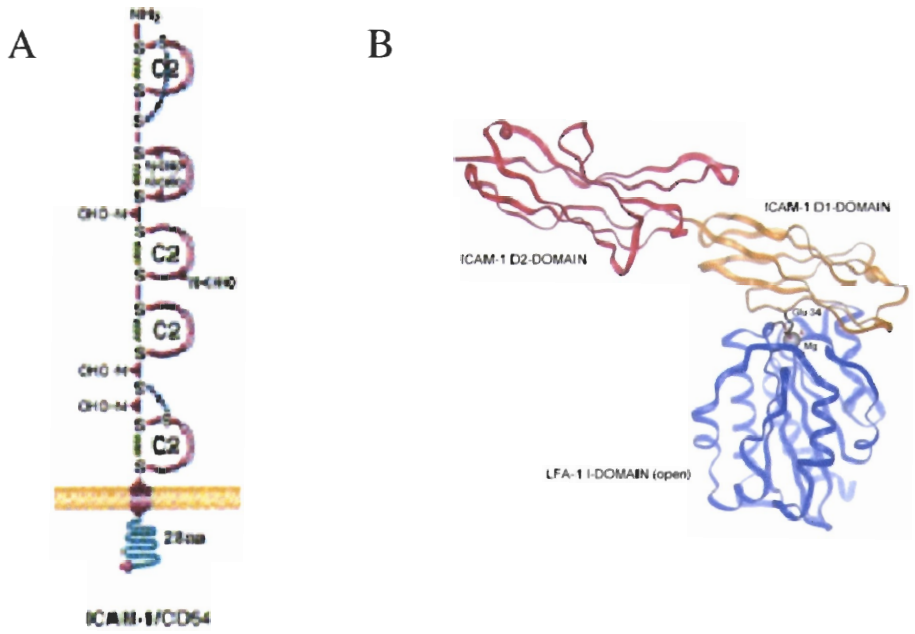

Figure 2-11. (A) Domain arrangement of ICAM-1. (B) The structure of D1-2 of ICAM-1 and the interaction between ICAM-1 and $\alpha_L\beta_2$. Glu-34 in D1 coordinate with Mg^{2+} (gray ball) in MIDAS of I domain.

Receptor-Ligand Binding Kinetics

Receptor-ligand interactions are usually modeled by using a chemical kinetics framework. For example, the following simple reversible reaction scheme between a free receptor R and a free ligand L to form a bond B:

$$R + L \underset{k_r}{\overset{k_f}{\leftrightarrow}} B \qquad \textbf{Equation 2-1}$$

where k_f and k_r are the respective forward rate (on-rate) and reverse rate (off-rate) constant. These kinetic rate constants are essential determinants of cell adhesion, for

these parameters describe how rapidly cells bind and how long they remain bound (Chesla *et al.*, 1998). The time rate of change of the bond concentration [B] is related to the free receptor concentration [R] and the free ligand concentration [L] through these constants:

$$\frac{d[B]}{dt} = k_f[R][L] - k_r[B] \qquad \textbf{Equation 2-2}$$

At equilibrium, $d[B]/dt = 0$. The free receptor, free ligand, and bond concentration are related through the dissociation constant, $K_d = k_r/k_f$,

$$K_d = \frac{[R][L]}{[B]} \qquad \textbf{Equation 2-3}$$

The affinity constant is K_a, $K_a = 1/K_d$.

Much progress has been made in recent years to determine some of the relevant adhesion parameters experimentally. There are many methods for measuring 3D receptor-ligand interaction kinetics when at least one of the molecular species is in solution. Examples are stop-flow experiments and surface plasmon resonance experiments (Gomes & Andreu, 2002). However, few techniques allow quantification its 2D counterpart, when the two species are bound to two apposed surfaces, as in the case of cell-cell or cell-extracellular matrix adhesion. Recently, several techniques and models have been developed to characterize of bonds formed between two apposing surfaces. Using quantitative fluorescent microscopy, 2D affinity of CD2 to LFA-3 was determined by Dustin *et al.* (1996) using cells resting on a glass-supported lipid bilayer. Chesla *et al.*

(1998) developed a model with a micropipette binding frequency assay for measuring the force-free 2D affinity and kinetic rates for several forms of the Fcγ receptor CD16a and its ligand IgG. This method is an extension of that of Evans (Evans *et al.*, 1991, 1995), which used an ultrasensitive red blood cell as a picoforce transducer to detect the adhesion mediated by a low number of receptor-ligand bonds (Figure 2-12). The measured adhesion frequency can be expressed as a function of the contact duration and kinetic rate constants,

$$P_a = 1 - \exp\{1 - m_r m_l A_c K_a (1 - \exp(k_r t))]\} \qquad \textbf{Equation 2-4}$$

where m_r and m_l are respective densities for receptor and ligand. The effective binding affinity ($A_c K_a$) and the reverse-rate (k_r) were extracted from the binding frequency data by iteratively reweighted nonlinear regression to this model. Since the exact contact area A_c could not be measured but controlled by the experimenter to remain a constant, the affinity is called effective binding affinity because A_c and K_a are lumped together.

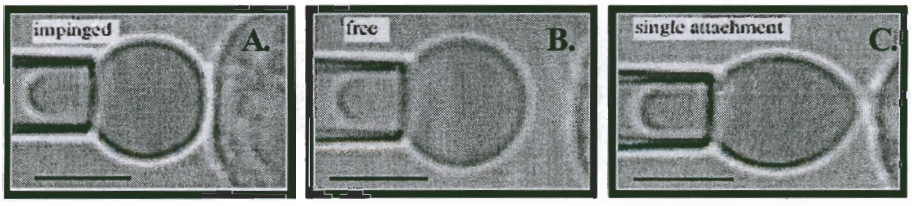

Figure 2-12. Photomicrographs of a typical adhesion test (Chesla *et al.*, 1998) (A) Two cells were brought into contact. (B) The unspirated portion of the RBC is shown in spherical shape. (C) The elongation of the bound RBC indicates an adhesion event.

This model assumes that binding occurs between a single receptor species and a single ligand species. However, various cell adhesion molecules often work together in

physiological conditions and affect adhesion and signaling simultaneously. They also have the potential to compete, cooperate, or cross-regulate with each other. To account for these *in vivo* situations, Zhu and Williams (2000) extended the previous model of Chesla *et al.* (1998) to include concurrent but independent interactions of multiple receptor-ligand species. The effective binding affinity (A_cK_{ai}) and the reverse rate (k_{ri}) of the ith species were extracted from the binding frequency data by iteratively reweighted nonlinear regression to the multi-species concurrent binding model (Equation 2-5),

$$P_a = 1 - \exp\{1 - \sum_{i=1}^{I} m_{ri} m_{li} A_c K_{ai} (1 - \exp(k_{ri} t))]\} \qquad \textbf{Equation 2-5}$$

where m_{ri} and m_{li} are the site densities of receptors and ligands for different species. Micropipette adhesion frequency assay has been proved to be an effective and reliable technique to measure the 2D binding kinetics of receptor-ligand interactions. Using this system, the binding kinetics of Fcγ receptor (Chesla et al., 1998), selectin (Long et al., 2001), and T cell receptor (Jiang et al., unpublished data) for their ligand have been characterized. It is also a useful tool to investigating biophysical and biological problems, such as the influence of anchoring form, molecule length, and glycosylation on 2D binding kinetics of receptors. Although this technique has been applied to study some function of integrins (Zhao et al., 2000), it has not been used for measuring integrin binding kinetics and for investigating the effects of conformational change and the divalent cation regulation of integrins.

CHAPTER III

MATERIALS AND METHODS

Cells Culture

K562 erythroleukemia cells stably transfected to express WT and mutatant α_L I domains or whole $\alpha_L\beta_2$ are kind gifts of Dr. T.A. Springer, Harvard Medical School (Lu *et al.,* 2001; Lu & Springer, 1997). Using human WT α_L I domain cDNA as a template, the mutations to cysteines (K287S and K294S for open I domain; L289S and K294S for closed I domain) were introduced to form conformation-specific disulfide bond. The WT and mutant I domains were fused to the platelet-derived growth factor receptor (PDGFR) transmembrane domain and the first five residues of the PDGFR cytoplasmic domain (Lu *et al.,* 2001). The cells were cultured in RPMI/10% fetal calf serum with glutamine (4 mM), penicillin/streptomycin (0.1 mg/ml). Hygromycin B (0.4 mg/ml) and puromycin (4 μg/ml) were used for selection agents for I domain and $\alpha_L\beta_2$, respectively. Maximum cell densities were ~$5x10^5$/ml.

Antibodies and Proteins

Purified mouse glycosyl phosphatidylinositol (GPI)-anchored ICAM-1 was a kind gift of Dr. P. Selvaraj, Emory University School of Medicine. To measure site densities of receptors and ligands in flow cytometry, mouse monoclonal antibody (mAb) DF1524 (anti-human CD11a) (Sigma-Aldrich, St. Louis, MO), rat mAb M1/70 (anti-human CD11b), mouse mAb 3.9 (anit-human CD11c), and rat fluorescein isothiocyanate

(FITC)-conjugated mAb YN1/1.7.4 (anti-mouse CD54) (eBioscience, San Diego, CA) were used. For negative controls, isotype-matched mouse and rat mAbs with no known human antigens were used, including MOPC-141 (Sigma-Aldrich), MOPC-21/P3, KLH/G2b-1-2 and FITC KLH/G2b-1-2 (eBioscience). Polyclonal goat anti-mouse IgG, conjugated to FITC (Sigma-Aldrich) and affinity purified goat anti-rat IgG, conjugated to FITC (Jackson Immunoresearch Laboratory, Inc., West Grove, PA) were used in flow cytometry as secondary antibodies for mouse primary antibodies. Blocking antibodies directed against ICAM-1 to $\alpha_L\beta_2$, $\alpha_M\beta_2$, and $\alpha_X\beta_2$ were 38 (Ancell Corporation, Bayport, MN), M1/70, and 3.9 (eBioscience), respectively.

Neutrophil Purification

Neutrophils for micropipette experiments were obtained from finger prick and that for flow cytometry was purified according to the following protocol. Approximately 5 ml of whole peripheral blood were drawn from healthy donors into sterile Vacutainers containing EDTA. The anticoagulated blood was mixed with half its volume of 6% Dextran 70 at room temperature and sat for 60 min. Supernant leukocyte-rich plasma was carefully collected and centrifuged at 350 rpm for 5 min at 4°C. 25 ml 2% NaCl was added to the pellet to lyse the red blood cells and the reaction was quenched after 20 seconds by adding 25 ml 1.6% NaCl. The mixture was centrifuged at 350 rpm for 5 min at 4°C. The pellet was resuspended in 5ml HBSS with 0.5% human serum albumin (HSA) and layered over 6ml of Histopaque 1119 (Sigma) and centrifuged at 350 rpm for 30 min at 4°C. Supernant was pipeted from polymorphonuclear leukocytes (PMN) pellet

by removing mononuclear leukocyte layer first, the RBC layer, then the HBSS/HSA layer, and finally the Histopaque layer. PMN pellet was resuspended in HBSS/HSA and cells were used for experiments immediately.

Isolation and Storage of RBC

RBCs were isolated from whole peripheral blood of healthy donors according to the following procedure (Williams *et al.*, 2001). Desired amount of whole blood was collected by venipuncture into sterile Vacutainers containing EDTA. The blood was mixed with equal volume of 0.85% saline and carefully layered over 3 ml of Histopaque 1119 (Sigma) and centrifuged at 700 g for 30 min at room temperature. The supernatant was removed and the pelleted erythrocytes were washed three times in RBC storage solution (EAS45) (Dumaswala *et al.* 1996). RBCs were stored in EAS45 at about 20% hematocrit at 4°C.

Reconstitution of GPI-ICAM-1 into RBCs

Low retention siliconized 1.5 ml Eppendorf tubes (Fisher Scientific International Inc., Hampton, NH) were coated with reconstitution buffer (PBS without magnesium and calcium, 1 mg/ml ovalbumin) overnight at 4°C or for 2 h at room temperature. Red blood cells were washed three times in reconstitution buffer and resuspended at 10^7 cells/ml. Desired volume of RBC suspension was added to the coated tubes into which purified mouse GPI-ICAM-1 was directly added at various concentrations. Reconstitution buffer was added to make the total volume 150 µl. Tightly sealed tubes were placed in a 37°C

incubator and gently rotated continuously on a rotator. After 2.5 h, RBCs were washed three times in ice cold EAS45 RBC storage solution. Reconstituted cells were analyzed by flow cytometry and stored at 4°C.

Flow Cytometry

Site Density Dertermination

Fluorescent staining

Staining for flow cytometry followed the standard protocol. Cells were washed in FACS buffer (RPMI with 1% FCS, 5mM EDTA, 0.02% Sodium Azide) and counted. $5x10^4$ cells were then resuspended in 100 µl FACS buffer and placed in a 1.5 ml Eppendorf tube. Samples were incubated on a shaker for 30 min at 4°C, with saturating concentrations of primary antibodies (usually 10 µg/ml of purified mAb or follow the manufacturer's instruction). For FITC-conjugated primary antibodies, cells were washed and analyzed immediately. For non-conjugated primary antibodies, FITC-conjugated anti-mouse IgG secondary antibody was added at saturating concentrations and the cells were incubated for an additional 30 min at 4°C in dark. Cells were then washed and analyzed immediately.

Data Acquisition

Samples were read on BD LSR flow cytometry (Becton-Dickinson Immunocytometry Systems, San Jose, CA) using FACS DiVa 3.1 software. Standard beads (Quantum™ 25 FITC High Level, Bangs Laboratory, Fisher, IN) were prepared for

quantification of MESF (molecules of equivalent soluble fluorophore). 2D gates of FL1 (FITC) histogram were created to gate on the forward scatter vs. side scatter histogram and placed around the singlet population to isolate single cells from aggregates and debris. These gates were created with the guidance of experience regarding the characteristic scatter patterns for single cells and aggregates of a particular cell type. The forward scatter thresholds were raised to exclude debris. FL1 (FITC) voltage levels were adjusted to place the fluorescent histograms of reference blank near the origin of the log intensity scale (Figure 3-1). After having established the calibration plot, no further adjustments were made to the instrument. The mean channels for each of the five calibrated microbeads were recorded. After completing the FI calibration procedure, the samples were run and the FL1 mean channels were recorded. Generally 10,000 events per sample were recorded.

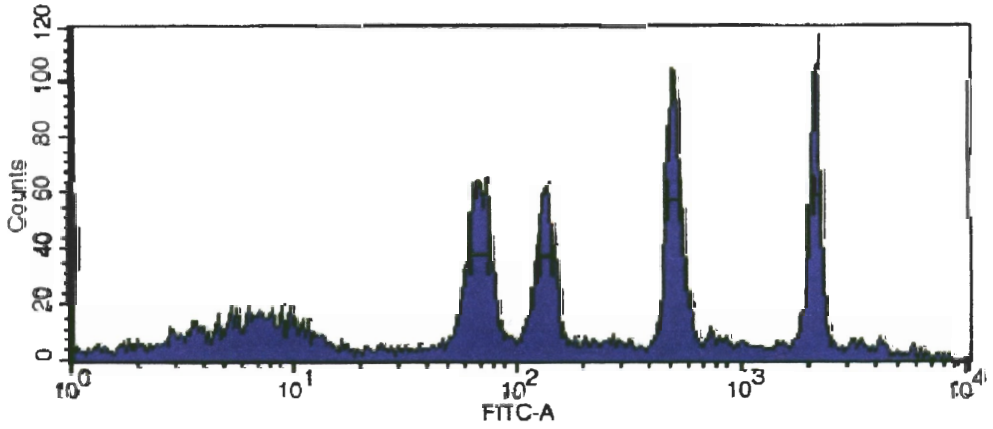

Figure 3-1. Fluorescent histograms of calibration beads. There are five peaks and the reference blank peak was put in the origin of the scale.

Data Analysis

The MESF (y-axis) vs. the RCN (relative channel number) (x-axis) for the five fluorescent micorbeads were plotted on a graph to obtain a calibration curve. The MESF value (corrected from the negative control) corresponding to the mean channel of each sample was read on the calibration curve. The site density of the molecule on cell surface was determined by dividing the MESF value by cell surface area and fluorine/protein ratio.

Cell Sorting

Fluorescent staining for cell sorting followed the same procedure as that for site density determination. Samples were read on BD FACSVantage SE flow cytometry (Becton-Dickinson Immunocytometry Systems, San Jose, CA). One of two gates was set at desired level of the log fluorescence intensity scale. The sorted cells were collected and the site densities were determined immediately after the sorting following the same procedure in site density determination. To achieve a high site density, cells need to be sorted multiple times at regular basis. Cell were replated and cultured for two weeks before the next sorting. As long as the desired site density was reached, the sorted cells were used for experiment after one or two day's culture.

Micropipette System

The micropipette system was designed, built, and calibrated in house (Chesla *et al.,* 1998). The system consists of video-enhanced optical microscopy,

micromanipulation, and pressure regulation subsystems (Figure 3-2). The centerpiece of the microscopic system is a Zeiss inverted microscope (Axiovert 100; Oberkochan, Germany) with a 100x oil immersion, 1.25 N.A. objective. Additional magnification is obtained using a 5x relay lens, leading to a charge-coupled device (CCD) camera (model 72S; Dage-MTI, Michigan City, IN). A digital image processor (model DSP-2000; Dage-MTI) is used to enhance the image. The signal also passes through a digital voltage multiplexer (model 401; Vista Electronics, Ramona, CA), which allows video integration and display of a timer on screen. Recording is accomplished using a super VHS video cassette recorder (model AG-7355; Panasonic, Secaucus, NJ).

Micropipettes were made from borosilicate glass tubing (O.D. 1mm) (World Precision Instruments, Inc.). A two-step process was used with the first, utilizing a micropipette puller (Model PN-30, Narishige, Japan). Next, a microforge (built in house, similar to commercial models, except that a glass bead is added to the filament, adapted from the laboratory of Robert M. Hochmuth, Duke University, Durham, NC) was used to break the micropipette with a flush tip at the desired diameter. Depending on the cell types, the openings of micropipettes vary from 2 to 10 μm inner diameter. The pipettes were connected to the pressure regulation system through stainless steel injection holders. Each pipette could be coarsely manipulated by a mechanical drive mounted on the microscope and finely positioned with a three-axis hydraulic micromanipulator (Narishige, Tokyo, Japan). In addition, one of the pipette holders was mounted on a piezo translator (Physik Instrumente, Waldbronne, Germany), the driver of which was controlled by a computer to achieve precise and repeatable movement of the pipette in an

adhesion test cycle. To avoid vibration of the micropipettes during the experiment, the microscope, along with the micromanipulators, was placed on an air suspension table (Kinetics Systems, Boston, MA). A pressure regulation subsystem was used to control suction during the experiment and was critical for tuning the sensitivity of the RBC picoforce transducer. A hydraulic line connected the micropipette holder to a fluid reservoir. The centerpiece of the design was a fine jack that allowed the height of the reservoir to be precisely manipulated.

Micropipette Binding Frequency Assay

The micropipettes were filled with HBSS without calcium and magnesium just before experiment. Chamber solution was HBSS without calcium and magnesium, 1% IgG-free bovine serum albumin (BSA), and 45-55% ddH_2O, mixed and sterile filtered just prior to use. For neutrophil experiments, 2% of human plasma (filtered prior to use) was added. For some experiments, 2 mM Mg^{2+}/2 mM EGTA (ethylene glycol-bis(2-aminoethylether)-N, N, N', N'- tetraacetic acid), or 2 mM Ca^{2+}, 2 mM Mn^{2+}, and/or 10 mM DTT was added to the chamber solution. Chamber was incubated with chamber medium for 30 minutes so that cells would not adhere to the bottom of chamber. One pipette was used to hold K562 cell or neutrophil and the other to hold a RBC. The two cells were aspirated gently and aligned with a small axial gap between them. One pipette was connected to a computer-controlled piezoelectric actuator that was programmed to move a prescribed distance at a uniform rate of 1 μm/sec. Cells would remain in contact for a prescribed duration and then retract. Background-subtracted images were viewed in

real time on a monitor and stored on videotape for future analysis (Chesla *et al.* 1998). This test cycle was repeated one hundred times with the same pair of cells, controlling the duration and area of the contact in these tests, and counting the numbers of adhesive events as adhesion frequency.

Data Analysis

Before extracting kinetics data, the nonspecific binding data were fitted to the equation,

$$P_{NS} = 1 - \exp[-a(1 - e^{-bt})] \qquad \textbf{Equation 3-1}$$

The specific binding probability P_a was determined by removing the fitted nonspecific data from the total adhesion frequency observed.

The effective binding affinity ($A_c K_a$) and reverse-rate (k_r) were extracted from the binding frequency data by iteratively reweighted nonlinear regression to the single-species model (Chesla *et al.*, 1998) (Equation 2-4) or to the multi-species concurrent binding model (Zhu & Williams, 2000) (Equation 2-5). The forward kinetic rate can be obtained from the relationship $K_a = k_f/k_r$. The adhesion frequency data (P_a) were fitted along with the known predictor variables (receptor and ligand surface site densities m_r and m_l, contact time t) (Figure 3-4).

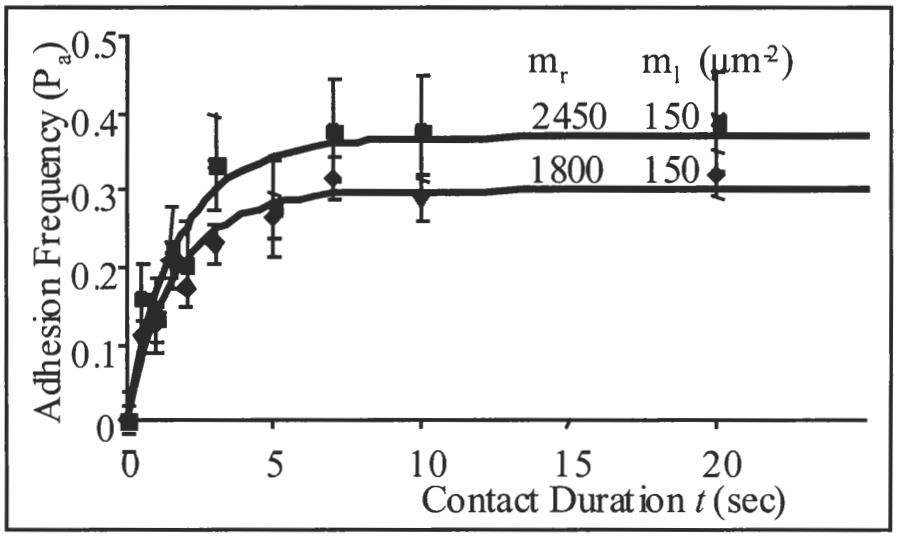

Figure 3-4. The dependence of adhesion frequency on contact duration and site densities of receptors and ligands. The adhesion frequency plotted as a function of the contact duration for each set of receptor and ligand densities, and fitted with the theoretical solution (Equation 2-4) (curves).

For some experiments, the adhesion frequency was measured for a constant contact duration and the effective binding affinity (A_cK_a) was estimated. When adhesion reached equilibrium, the effective affinity was estimated from the following equation,

$$A_c K_a = \frac{1}{m_r m_l} \ln(1 - P_a)^{-1} \qquad \textbf{Equation 3-2}$$

which is derived from the steady state version (i.e. $t \rightarrow \infty$) of Equation 2-4.

CHAPTER IV

2D BINGDING KINETICS OF ICAM-1 FOR ISOLATED α_L I DOMAINS AND THE REGULATION BY DIVALENT CATIONS

Introduction

Recent crystal structure studies revealed the open and closed conformations of the I domain and the 3D binding kinetics assay showed that these two conformations respectively correspond to high and low affinities differing by 9000 folds (Lu *et al.,* 2001; Shimaoka *et al.,* 2001). However, since the SPR experimental setup requires one of the binding partner, either the I domain or the ICAM-1 to be soluble in the medium flowing over the surface, the obtained kinetic rates were for soluble molecules on 3D kinetics. Although there is soluble ICAM-1 in blood stream, almost all the $\alpha_L\beta_2$-mediated functions are facilitated by binding to cell surface ICAM-1, e.g. on endothelium cells. Therefore, it is important to know whether the conformational changes of I domain could regulate the 2D binding affinity, which better resembles the physiological situation. However, the conversion of 3D kinetics into 2D kinetics is an unsolved issue (Dustin *et al.,* 2001).

Here, we characterized the 2D binding kinetics of ICAM-1 on RBC to the WT I domain and locked open and locked closed I domain mutants expressed on K562 cells, using the micropipette adhesion frequency assay. The locked open I domain showed an 8000-fold increase in binding affinity compared to locked close I domain and a 3000-fold increase compared to WT. The reverse rates of the three I domains are similar and thus

the increase in affinity was mostly contributed by the increasing of forward rates.

I domain-mediated binding is divalent cation dependent. Divalent cations have long been known to be universally required for ligand binding by integrins. In I domains, the metal-coordinating residues and the residues surrounding the metal-binding site, are important for ligand binding. Divalent cations may affect the binding by directly participating in binding to ligand, or by other indirect regulating mechanisms. It has been suggested that the Mg^{2+} or Mn^{2+} may be needed for stabilizing the high affinity structure of I domain (Qu & Leahy, 1996). Divalent cation binding is mediated by the conserved DXSXS sequence, residues 131-135 in α_L I domain and homologous regions in other I domains, T206 and D239 of α_L and their equivalent in other I domains (Qu & Leahy, 1996).

We measured the affinity change caused by divalent cations on I domains. The open and closed I domain locked by disulfide bonds were not regulatable by Mg^{2+}, Mn^{2+} and Ca^{2+}. For wild type I domain, the binding was upregulated by Mg^{2+} or Mn^{2+} by less than 2 folds; however, Ca^{2+} at mM concentration did not affect the binding mediated by wild type I domain. DTT treatment, which released the disulfide bond and presumably allowed the locked I domain to return to the WT conformation, dramatically reduced the ICAM-1 binding of the locked open I domain and increase the binding of the locked closed I domain slightly. Moreover, they became regulatable by divalent cations. These data suggest that the locked conformations are required for the respective high and low affinities, and cations alone are insufficient for high affinity interaction.

Results

Cell sorting and site densities of I domains

The site densities of I domains and ICAM-1 were adjusted so that the adhesion frequency fall into the mid range between 0 and 1. Moreover, the site densities were varied to generate several curves for reliable analysis. K562 cells were sorted before each experiment to adjust the site densities of I domains. The site densities of ICAM-1 were also adjusted by varying the volume of purified ICAM-1 added during reconstitution.

Divalent cations requirement for I domain-ICAM-1 interaction

Initial micropipette experiments using K562 cells respectively expressing open I domain, closed I domain, and WT I domain were carried out in HBSS- medium in the absence or presence of 5 mM EDTA. Binding was completely abolished by EDTA for all three I domains (Figure 4-1). Two-sided student-*t* test showed that the difference between the adhesion when measured in HBSS- with and without EDTA was statistically significant (P-value = 0.0002). The fact that the cells in HBSS- could still bind ICAM-1 indicated that there were trace amount of divalent cations existed in the medium even when HBSS- was used.

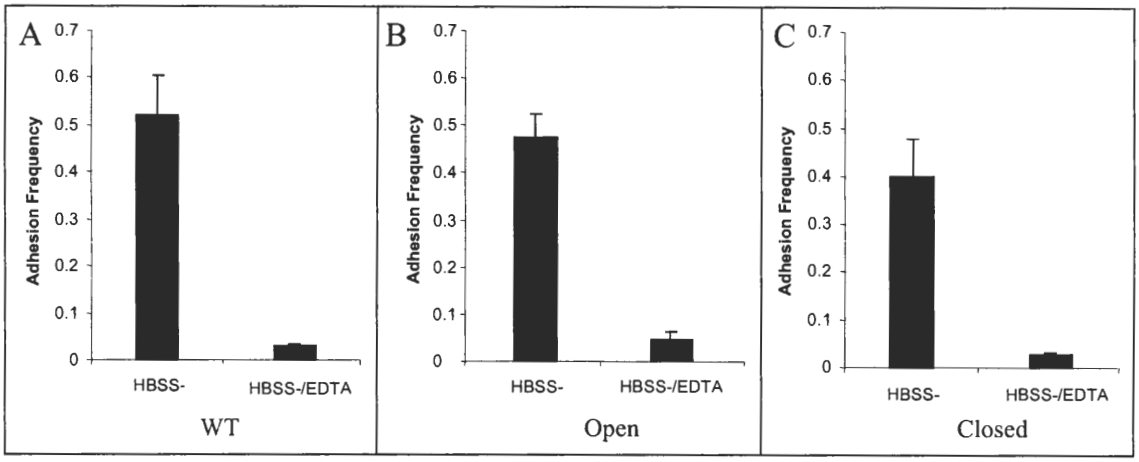

Figure 4-1. Respective adhesion frequencies of (A) WT, (B) open, and (C) closed I domain to ICAM-1 with HBSS- in the absence or presence of EDTA. Data were presented as mean ± standard error of the mean (S.E.M.) of 5 pairs of cells each contacting 100 times to estimate the adhesion frequency. The same densities of I domain and ICAM-1 were used in the same panel, which were varied from panel to panel to obtain mid-ranged adhesion frequency for the condition without EDTA.

Binding Kinetics of I domains to ICAM-1

Subsequent micropipette adhesion frequency assays were carried out to measure the ICAM-1 binding kinetics of I domains. For each I domain, 2 to 4 binding curves were generated by varying the site densities of I domains and ICAM-1 (Figure 4-2). The kinetic rates extracted from different curves of the same species are similar (Figure 4-3, Table 4-1). The locked open I domain showed an 8000-fold increase in binding affinity compared to the closed I-domain and a 3000-fold increase compared to WT (Figure 4-3A). The reverse rates (k_r) of the three I domains were similar (Figure 4-3B), which indicates that the increase in affinity is due mostly to the increases in the forward rates (k_f).

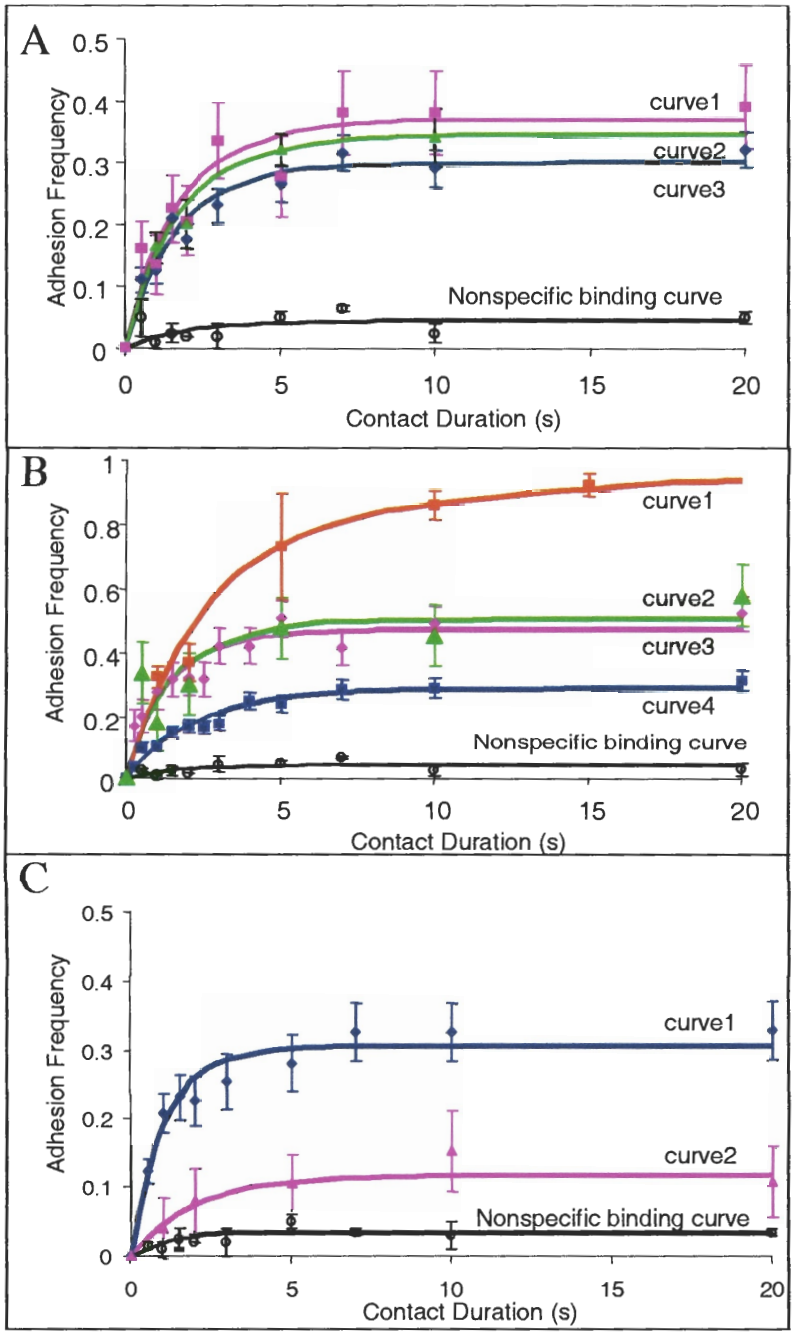

Figure 4-2. ICAM-1 binding curves for I domains. (A) WT I domain. (B) locked open I domain. (C) locked closed I domain. Each point represents mean adhesion frequency ± S.E.M. of 3 pairs of cells with 100 contacts each. Curves indicate best-fit solutions to the adhesion frequency binding model of Chesla *et al.* (1998).

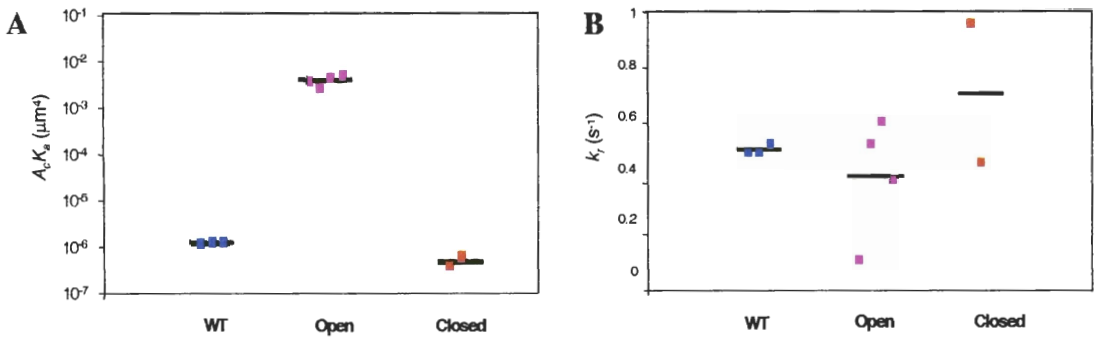

Figure 4-3. 2D kinetic rates of WT, open and closed I domains for ICAM-1 extracted from the binding curves in Figure 4-4. Each point represents (A) the effective affinity or (B) the reverse rate extracted from one curve. Bars represent average values.

Table 4-1. List of site densities and kinetic constants of the corresponding binding curves of I domains in Figure 4-4.

		I domain (μm^{-2})	ICAM-1 (μm^{-2})	$A_c K_a$ (μm^4)	$A_c k_f$ ($\mu m^4 \cdot s^{-1}$)	k_r (s^{-1})
WT	curve1	2450	150	1.25E-6	6.25E-7	0.50
	curve2	2700	115	1.35E-6	6.75E-7	0.50
	curve3	1800	150	1.32E-6	6.70E-7	0.53
	Average ± S.E.M.			1.31(±0.03) E-6	6.57(±0.16) E-6	0.51(±0.01)
Open	curve1	17	44	3.97E-3	4.37E-4	0.11
	curve2	8	32	2.73E-3	1.45E-3	0.53
	curve3	7	20	4.57E-3	2.79E-3	0.61
	curve4	7	9	4.92E-3	1.72E-3	0.40
	Average ± S.E.M.			4.05(±0.48) E-3	1.60(±0.49) E-3	0.41(±0.11)
Closed	curve1	2500	300	4.03E-7	3.87E-7	0.96
	curve2	1775	115	6.12E-7	2.82E-7	0.46
	Average ± S.E.M.			5.07(±1.04) E-7	3.35(±0.53) E-7	0.71(±0.25)

The regulation of WT I domain by Mg^{2+}, Mn^{2+} and Ca^{2+}

WT I domain was regulatable by divalent cations. The binding affinity of WT I domain was significantly (student-*t* test, P-value = 0.01) increased by Mg^{2+} or Mn^{2+} by ~ 2 folds (Figure 4-4A; Table 4-2). However, Ca^{2+} did not inhibit the binding of WT I domain (student *t* test, P-value=0.90) (Figure 4-4A; Table 4-2).

The lack of regulation of the locked open/closed I domains by Mg^{2+}, Mn^{2+} and Ca^{2+}

The binding affinities of locked I domains measured in HBSS- with or without Mg^{2+}/EGTA, Mn^{2+}, or Ca^{2+} were measured. To ensure the equivalent I domain site density, the same population of K562 cell after sorting were used for the experiments with different treatments. RBC was also from the same batch of preparation. The addition of divalent cations did not affect the binding of the locked I domains (Figure 4-7B, C; Table 4-1). Two-sided *t* test showed that there is no statistically significant difference between the binding affinities of locked I domains measured in HBSS- and Mg^{2+} (P-value = 0.73), between HBSS- and Mn^{2+} (P-value = 0.74), and between HBSS- and Ca^{2+} (P-value = 0.90).

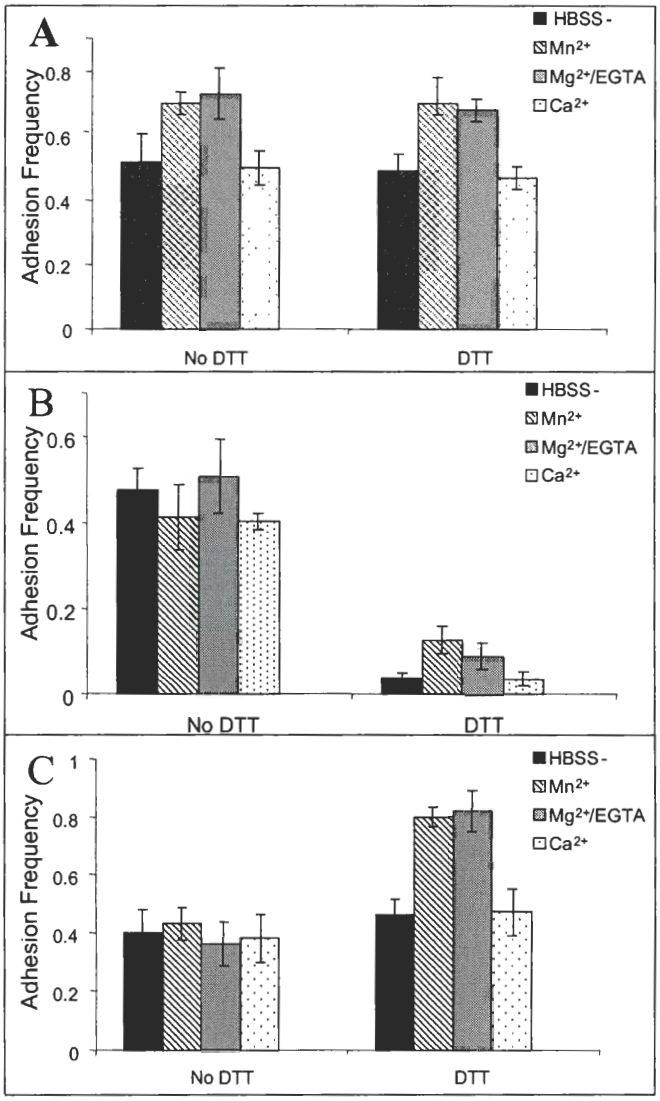

Figure 4-4. Changes in steady state adhesion frequency of (A) WT I domain, (B) open I domain, and (C) closed I domain to ICAM-1 when treated with the indicated agents. Data were presented as mean ± S.E.M. of 5 pairs of cells each contacting 100 times to estimate the adhesion frequency. The same I domain and ICAM-1 densities were used in the same panel but were different in different panels to obtain mid-range adhesion frequencies. The contact duration was set to be 10 seconds, which should yield steady state adhesion frequency based on the binding curve data shown in Figure 4-2.

Table 4-2. Effective affinities of the WT and locked I domains when treated with indicated agents. Equation 3-2 was used to estimate effective affinities from the adhesion frequency data in Figure. 4-7.

			A_cK_a (μm^4)			
	I domain (μm^{-2})	ICAM-1 (μm^{-2})	HBSS-	Mn^{2+}	Mg^{2+}/EGTA	Ca^{2+}
WT	2750	200	1.35E-6 ±0.09E-6	2.42E-6 ±0.19E-6	2.27E-6 ±0.18E-6	1.27E-6 ±0.11E-6
Open	7	20	3.11E-3 ±0.36E-3	2.82E-3 ±0.49E-3	3.31E-3 ±0.27E-3	3.07E-3 ±0.38E-3
Closed	2500	300	5.81E-7 ±0.68E-7	5.26E-7 ±0.92E-7	6.17E-7 ±0.42E-7	5.74E-7 ±0.70E-7

The reduction of disulfide bonds released the mutant I domains locked in the open and closed conformation into wild type conformation

To ensure that the difference in binding affinities requires the presence of the disulfide bonds, cells were treated with DTT prior to and during the micropipette experiments. DTT did not affect the binding of WT I domains (Figure 4-7A). However, it reduced the binding of the open I domain to background level (Figure 4-7B). Although not statistically significant (student-*t* test, P-value = 0.29), DTT treatment slightly increased the affinity of the locked closed I domain (Figure 4-7C). After the reduction of disulfide bonds, locked open and closed I domains became upregulatable by Mg^{2+} and Mn^{2+}, which significantly increased the binding of the reduced open and closed I domains (student-*t* test, P-value = 0.01 for both reduced open and closed I domains) (Figure 4-7B,C).

Discussion

Using micropipette adhesion frequency assay, we measured the 2D binding kinetics of the isolated wild type and mutant I domains to ICAM-1. This interaction requires divalent cation, as EDTA completely abolished the binding. The affinity of the locked open I domain showed an 8000-fold increase relative to the locked closed I domain. The affinity of WT I domain was only ~ 2 fold higher than the locked closed I domain for ICAM-1.

In contrast to SPR measurements, which determine the 3D kinetics, the micropipette assay estimates the binding kinetics of cell surface bound molecules. The 8000-fold increase seen in our experiment is in good agreement with the 9000-fold increase obtained from the SPR experiment. This indicated that the conformational changes substantially altered the ligand binding affinity of the I domains on cell membrane to the same extent as that in the 3D situation. Both SPR and our micropipette data suggested that the dramatic difference in binding affinity is mainly due to the forward rate (Shimaoka *et al.*, 2001). This is consistent with the notion that conformational change is the rate-limiting step for binding of the wild type I domain. However, our data showed only ~ 2 folds difference between the reverse rates of the locked open and locked closed I domains, whereas 3D data showed a 100-fold difference (shimaoka *et al.,* 2001). There has not been a definite explanation for this discrepancy; however, the difference in the way the proteins were presented (soluble vs. cell membrane bound) and the difference in the experimental system (SPR vs. micropipette) could contribute to this discrepancy.

The increased affinity of the locked open I domain relative to the locked closed I domain required the presence of disulfide bonds, because the reduction of disulfide bond by DTT substantially reduced the ligand binding activity of the open I domain. Since we used low densities of open I domain and ICAM-1 to achieve mid range binding, the adhesion frequency after DTT treatment was reduced to background level, preventing us from estimating the binding affinity. However, other studies showed that the affinity of the DTT treated open I domain was comparable to that of the wild type and locked closed I domain (Shimaoka *et al.,* 2001; Lu *et al.,* 2001). This finding plus the fact that the binding kinetics of wild type and locked closed I domain are comparable, indicating that on rest cells, wild type I domain exists in the low affinity (closed) conformational state, which is strongly favored by its lower energy (Lu *et al.,* 2001; Shimaoka *et al.,* 2000).

Not only do the kinetic measurements of the isolated I domains reveal the importance of the conformational change in I domain affinity regulation but they also provided evidence for an I domain activation pathway. Since the position of the introduced disulfide bond is far away from the ligand-binding site, the only way it could affect the affinity would be allosteric regulation by restraining the conformation and position of the β6-α7 loop and the α7 helix (Shimaoka *et al.,* 2002). Our results clearly demonstrated that the reposition and reshape of this helix and the preceding loop could affect the conformations of the binding site, MIDAS. Thus, in intact integrins, a downward pulling on the C-terminal a-helix of the I domain exerted by neighboring domains could be sufficient to open the ligand binding site.

As an important player in integrin regulation, divalent cation also affects the

binding of the isolated I domains. The coordination of Mg^{2+} or Mn^{2+} has dramatic effects on the shape and electrostatic properties of the MIDAS (Qu & Leahy *et al.,* 1995). We observed that Mg^{2+} and Mn^{2+} increased the binding of WT I domain to ICAM-1 by 2 folds. Since Mg^{2+} or Mn^{2+} participates in the ligand binding by coordinating the residues in correct position, the observed ICAM-1 binding is proportional to the fraction of the I domain bound with Mg^{2+} or Mn^{2+} (Labadia *et al.,* 1998). Thus, higher concentration of Mg^{2+} or Mn^{2+} increases the binding affinity of WT I domain by increasing the fraction of the I domain bound with Mg^{2+} or Mn^{2+}. However, since the conformation of mutated I domains were locked and thus unable to undergo the conformational change, their binding was not changed by Mg^{2+} or Mn^{2+}.

High concentration of Ca^{2+} is known to be inhibitory against many integrins containing an I domain. However, our data showed that Ca^{2+} at mM concentration did not inhibit the binding of WT I domain to ICAM-1. This is consistent with previous studies showing that the binding of isolated α_2 (Oxvig *et al.,* 1999) and α_L I domains (Shimaoka *et al.,* 2002) to their ligands was not inhibited by Ca^{2+}. It appears that the Ser and Thr side chains in the MIDAS strongly disfavor Ca^{2+} coordination (Shimaoka *et al.,* 2002). A study of divalent cation binding to the recombinant I domain exploited Tb^{3+}, a fluorescent probe of protein divalent cation-binding sites, to examine the relative affinities of the I domains for divalent cations. It has been demonstrated that Ca^{2+} did not compete with Tb^{3+} for binding and the I domain divalent cation binding site prefers Mg^{2+} and Mn^{2+} (Dickeson & Santoro, 1998). However, Griggs *et al.* (1998) suggested that α_L I domain contains a Ca^{2+} binding site and Ca^{2+} antagonism of $\alpha_L\beta_2$ mediated cell adhesion may be

a consequence of Ca^{2+} binding activity of the I domain. Therefore, further studies may be necessary to investigate the effects of Ca^{2+} to the isolated I domain and whole integrin.

CHAPTER V

2D BINDING KINETICS OF ICAM-1 FOR $\alpha_L\beta_2$ AT DIFFERENT CONFORMATIONAL STATES AND THEIR REGULATION BY DIVALENT CATIONS

Introduction

The I domain locked in open conformation showed a dramatic increase in binding affinity either in soluble or cell membrane bound form. However, it is not known whether the locked open I domain assumes the conformation of physiological high affinity I domain and whether it is sufficient for ligand binding. Both our and other's data showed that the binding of the isolated wild type α_L I domain on K562 cells to immobilized ICAM-1 is only detected when the I domain and ICAM-1 were at high site densities (Chapter IV; Knorr & Dustin, 1997). Furthermore, Mg^{2+} or Mn^{2+} only increased the affinity of WT I domain by ~ 2 fold (Chapter IV). Therefore, it appears that the isolated I domain alone might not be sufficient to mediate strong and stable interaction with ligand. If the bell-rope-like pull model for I domain activation is correct, it is expected that other domains contact with I domain exert this pulling down.

To address the above issues, we measured the binding kinetics of wild type intact $\alpha_L\beta_2$ on K562 cell to ICAM-1 on RBC and compared the kinetic rates with those of the K562 cell isolated α_L I domain. The $\alpha_L\beta_2$ was either activated by Mg^{2+} or Mn^{2+}, or inactivated by Ca^{2+} or without metal ion treatment (HBSS-). The binding affinity of intact $\alpha_L\beta_2$ in HBSS- was 5 folds higher than that of the wild type I domain. Treatment with

Mg^{2+} (or Mn^{2+}) increased the binding affinity increased ~335 (or 1140) folds, resulting a value comparable to that of the locked open I domain. Ca^{2+} treatment decreased the binding affinity by 2 folds. Thus, the range of affinity regulation by divalent cations for whole $\alpha_L\beta_2$ approached that of the affinity difference between the isolated locked open and closed I domains. Our data suggest that the isolated open I domain alone is sufficient for ligand binding and the I domain in intact integrin could be activated by the downward pull by other domain, such as I-like domain.

Results

Divalent cation requirement for the binding of intact $\alpha_L\beta_2$

Similar to the isolated I domain, the binding of intact $\alpha_L\beta_2$ to ICAM-1 also required on divalent cations. The cells were washed with HBSS containing EDTA prior to experiment and the adhesion was reduced to the background level (Figure 5-1).

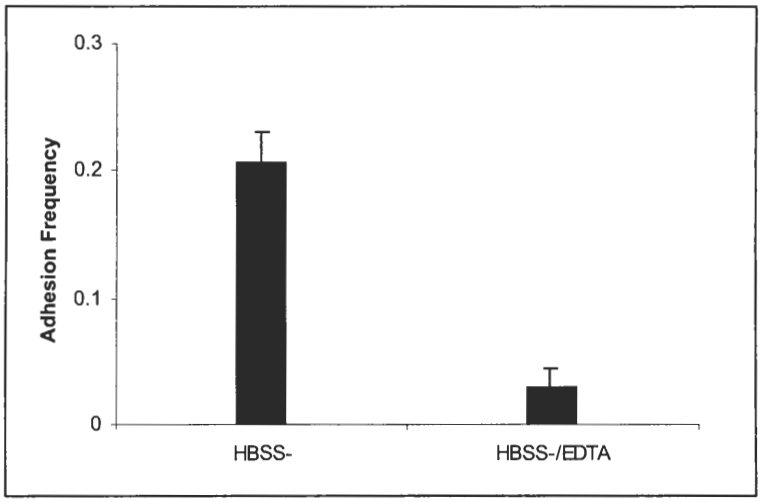

Figure 5-1. Adhesion frequency of wild type $\alpha_L\beta_2$ measured in HBSS- with or without EDTA. Data were presented as mean ± S.E.M. of 5 pairs of cells each contacting 100 times to estimate the adhesion frequency.

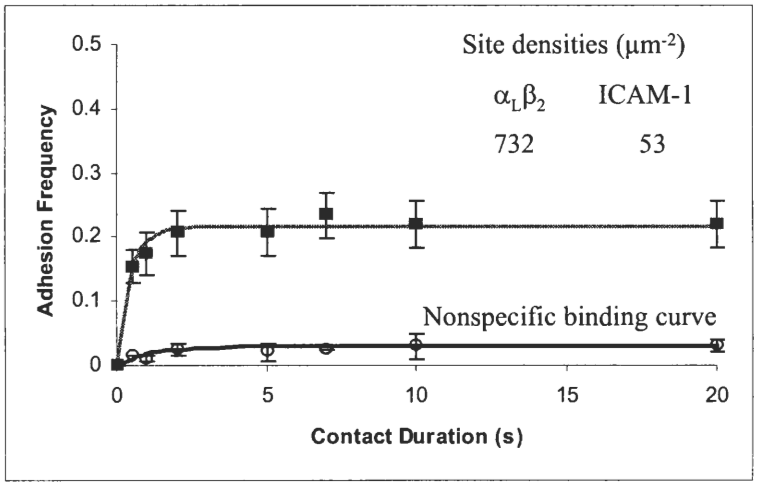

Figure 5-2. ICAM-1 binding curves for WT $\alpha_L\beta_2$ measured in HBSS-. Each point represents mean adhesion frequency ± S.E.M. of 3 pairs of cells with 100 contacts each. Curves indicate best-fit solutions to the adhesion frequency binding model of Chesla *et al.* (1998).

Binding kinetics of intact $\alpha_L\beta_2$ on K562 cells

The site densities of $\alpha_L\beta_2$ and ICAM-1 were adjusted to obtain mid-ranged adhesion frequencies. The kinetic rates of intact $\alpha_L\beta_2$-ICAM-1 interactions were extracted from the binding curves (Figure 5-2). Table 5-1 summarizes the effective affinities and reverse rates of wild type $\alpha_L\beta_2$ measured in HBSS with Mg^{2+}/EGTA.

Table 5-1. The kinetics rates of wild type $\alpha_L\beta_2$ measured in indicated agents.

	$\alpha_L\beta_2$ (μm^{-2})	ICAM-1 (μm^{-2})	A_cK_a (μm^4)	k_r (s^{-1})
HBSS-	732	53	6.18(±0.02) E-6	2.07±0.66
Mg^{2+}/EGTA	21	14	2.07(±0.07) E-3	0.53±0.19
Mn^{2+}	21	14	7.04(±1.22) E-3	--
Ca^{2+}	732	53	3.30(± 0.64) E-6	--

The regulation of WT $\alpha_L\beta_2$ by Mg^{2+}, Mn^{2+} and Ca^{2+}

Binding affinity of Mg^{2+} activated $\alpha_L\beta_2$ was ~ 335 folds higher than that measured in HBSS- only (Figure 5-3; Table 5-1) and it was comparable to that of the locked open I domain (Figure 5-6). The difference in the reverse rates was ~ 4 folds. To further investigate the effects of divalent cations on $\alpha_L\beta_2$ binding, the steady-state adhesion frequencies of $\alpha_L\beta_2$ with Mn^{2+} and Ca^{2+} were measured at a constant contact time of 10 seconds and the binding affinities were estimated from Equation 3-2 (Table 5-1). The adhesion frequencies of wild type $\alpha_L\beta_2$ with HBSS-, or with Ca^{2+} are shown in Figure 5-4. Ca^{2+} decreased the binding affinity by ~ 2 folds. When using high site densities of $\alpha_L\beta_2$ and ICAM-1, Mg^{2+} and Mn^{2+} increased the adhesion frequency into 1 and it is impossible to estimate any kinetics rate; therefore, cells with low site densities of $\alpha_L\beta_2$ and ICAM-1 were used for those experiments. The adhesion frequencies are shown in Figure 5-5 and the binding affinities estimated are listed in Table 5-1. Known as a strong activator for integrin, Mn^{2+} increased the binding affinity of $\alpha_L\beta_2$ by 3 folds more

than Mg^{2+}, which means that Mn^{2+} is more potent for activating whole integrin than Mg^{2+}.

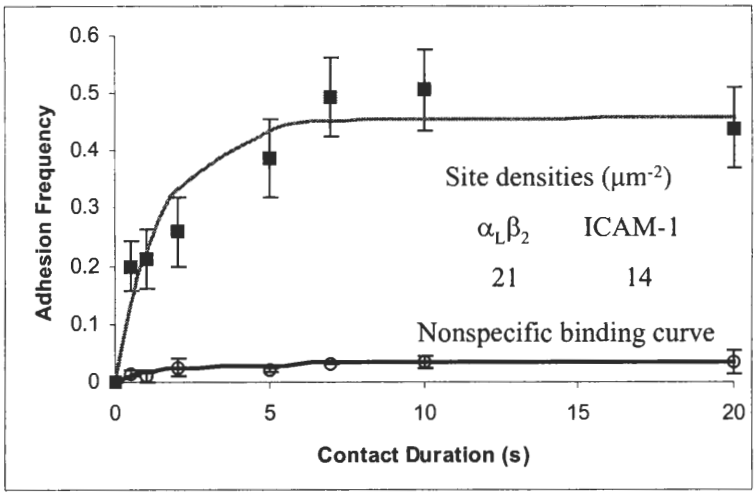

Figure 5-3. ICAM-1 binding curves for WT $\alpha_L\beta_2$ measured in Mg^{2+}. Each point represents mean adhesion frequency ± S.E.M. of 3 pairs of cells with 100 contacts each. Curves indicate best-fit solutions to the adhesion frequency binding model of Chesla *et al.* (1998).

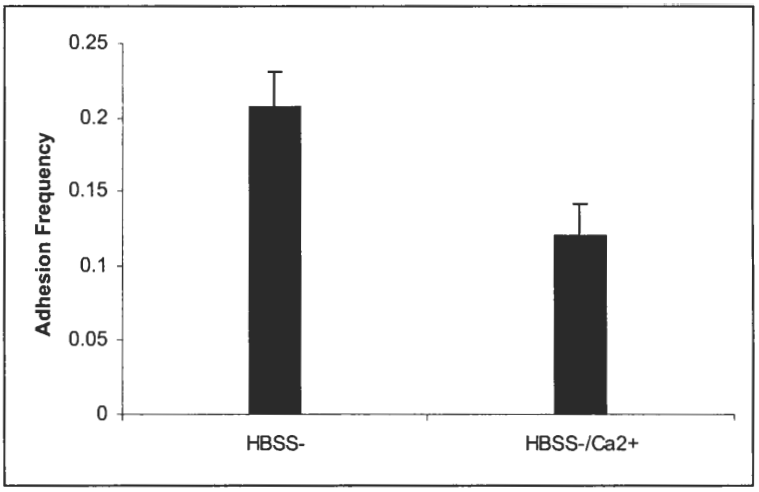

Figure 5-4. Adhesion frequency of wild type $\alpha_L\beta_2$ with or without Ca^{2+}. Data were presented as mean ± S.E.M. of 5 pairs of cells each contacting 100 times to estimate the adhesion frequency.

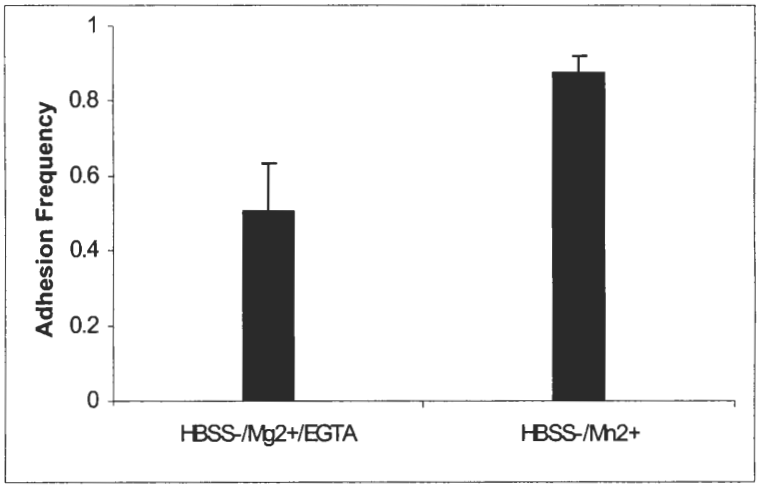

Figure 5-5. Adhesion frequency of wild type $\alpha_L\beta_2$ with Mg^{2+}/EGTA and with Mn^{2+}. Data were presented as mean ± S.E.M. of 5 pairs of cells each contacting 100 times to estimate the adhesion frequency.

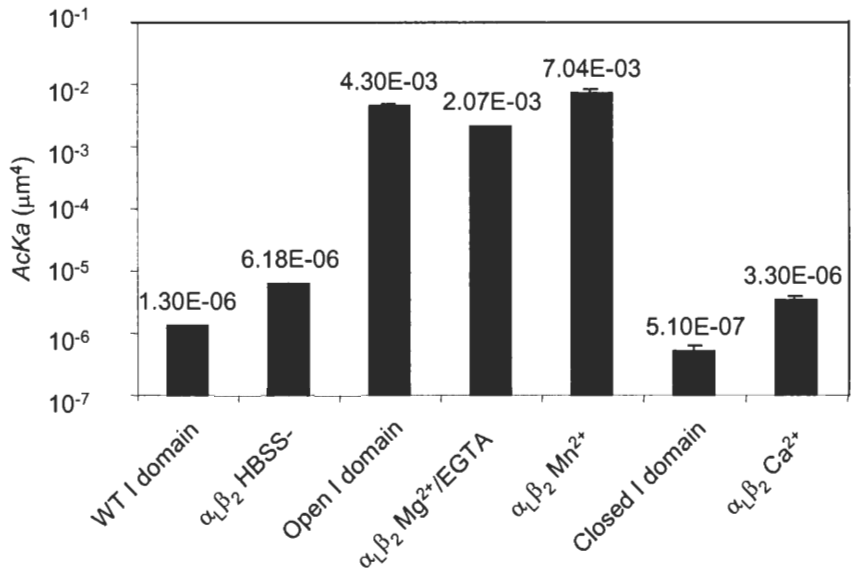

Figure 5-6. Comparison of the effective affinities of isolated I domains and intact $\alpha_L\beta_2$. The isolated I domains were measured in HBSS- and $\alpha_L\beta_2$ was measured in HBSS- with or without the indicated agents. The binding affinities are presented as mean ± S.E.M.

Discussion

The binding affinity of WT $\alpha_L\beta_2$ was 5 folds higher than that of the WT isolated I domain when measured in HBSS-. Previous work using a GPI-anchored, isolated wildtype α_L I domain has also shown that ligand binding by the isolated I domain is much weaker than that by the intact integrin (Knorr & Dustin, 1997). Without other stimulations, wild type I domain as well as wild type intact integrin are likely to be in inactive state with low binding affinity (Shimaoka *et al.,* 2001; Lu *et al.,* 2001). Physiologically, it has been suggested that integrins assume multiple conformational states that coexist in equilibrium rather than being locked in a single conformation (Luo *et al.*, 2003). Both signaling inside the cell and ligand binding will affect the equilibrium.

Therefore, there are always integrins existing in either high or intermediate affinity state and ready for ligand binding. Since the cells were supplied with divalent cations during culture, there was trace amount of Mg^{2+} that were already bound to the integrins even though HBSS- was used as chamber medium. After the cells were washed with HBSS containing EDTA before experiment, the ICAM-1 binding of intact $\alpha_L\beta_2$ was reduced to background level (Figure 5-1). It is expected that the Mg^{2+} would favor the conformational change of some $\alpha_L\beta_2$ integrins into active state. The ligand binding could further induce outside-in signaling and activate other integrins (Hynes 2002; Shimaoka *et al.,* in press). However, for the isolated I domain, the conformational change induced by ligand binding is unlike to be propagated into cell through a PDGFR transmembrane domain.

The I domain deleted $\alpha_L\beta_2$ showed no recognition of ligands, confirming the essential role of the I domain in ligand binding (Leitinger & Hogg, 2000). Both SPR measurements (Shimaoka *et al.,* 2001; Labadia *et al.* 1998) and our data showed that the binding kinetics of locked open I domain and the active $\alpha_L\beta_2$ are comparable. It indicated that the locked open I domain alone is sufficient for ligand binding on cell surface and that the locked open conformation of I domain corresponds to the physiologically open conformation in active integrins. The conformational change in I domain might be the final and most important step for regulating binding affinity of whole integrin, since the affinity of Mg^{2+} activated $\alpha_L\beta_2$ was even slightly lower than that of the locked open I domain.

Mg^{2+} and Mn^{2+} activated both the WT $\alpha_L\beta_2$ and the isolated WT I domain. Mg^{2+}

increased the binding affinity of $\alpha_L\beta_2$ by > 300 folds; while only increased the affinity of I domain by < 2 folds. Mn^{2+} had higher efficacy for activating $\alpha_L\beta_2$, but has the same effect on I domain as Mg^{2+}. These further confirms the importance of other domains in regulating the activity of the I domain. The activation may occur by downward pull of the C-terminal of the I domain as is proposed by Carman & Springer (in press). It is not clear how Mg^{2+} affect the conformation of whole integrin regarding to the switchblade-like global conformational change. However, there are at least two coordinating sites for Mg^{2+}, the MIDAS in I domain and in I-like domain (Shimaoka *et al.,* 2003; Kamata *et al.,* 2002; Takagi *et al.,* 2002). It is suggested that Mg^{2+} does not induce inside-out signaling (Arroyo *et al.,* 1992; Leitinger *et al.,* 2000), and thus Mg^{2+} activates integrin by outside-in signaling through regulating the conformation of I domain or I-like domain. Therefore, our data suggested that the propagation of ligand binding induced conformational change as well as the activation of integrins through this signaling is also dependent on the interdomain movement. For many integrins, ligand recognition is augmented by the presence of Mn^{2+}. However, the basis of this phenomenon is poorly understood. Our data showed that Mn^{2+} further increased the binding affinity of $\alpha_L\beta_2$ compared to Mg^{2+}. This may due to the global conformational change of the integrin, because Mn^{2+} is known to stabilize an extended intermediate affinity conformation of integrin (Shimaoka *et al.,* in press). However, it is not clear whether Mg^{2+} also be able to induce this extended conformation of integrin, so the difference between the effects of Mg^{2+} and Mn^{2+} to integrin binding may be caused by other factors, such as inside-out signaling.

CHAPTER VI

2D BINDING KINETICS OF ICAM-1 FOR THREE NEUTROPHIL β_2 INTEGRINS

Introduction

The erythroleukemia cell line K562 transfected to express I domains and intact $\alpha_L\beta_2$ represent a simple and relevant model for the aims of this study. To test the results obtained with the K562 cells in a more complicated and perhaps more physiological system, we performed micropipette experiments using human neutrophils. Neutrophils are the most abundant type of leukocytes in humans that constitutively express at least three ICAM-1-binding β_2 integrins, $\alpha_L\beta_2$, $\alpha_M\beta_2$, and $\alpha_X\beta_2$. The attachment of neutrophils to the vascular endothelium and their passage to sites of inflammation involves a sequence of events including neutrophil tethering, rolling, and firm adhesion (Laurence & Springer, 1991). The firm adhesion is dependent on members of the β_2 integrins after activation by intracellular signaling. While many details of the β_2 integrin-mediated adhesions continue to emerge, direct measurements of 2D binding kinetic rates and the regulation by divalent cations have not been reported. Knowledge of the kinetics of neutrophil β_2 integrin under different conformation states induced by divalent cations will help us better understand their role in immune and inflammation responses. It may also provide new insights into the physiologically relevance of the proposed model for β_2 integrin activation.

The 2D binding kinetics of ICAM-1 for $\alpha_L\beta_2$, $\alpha_M\beta_2$, and $\alpha_X\beta_2$, were measured

using micropipette frequency assay in the presence or absence of Mg^{2+}/EGTA and/or Ca^{2+}. Kinetics rates were extracted from the measured binding curves. Mg^{2+} increased the binding affinity of β_2 integrins to ICAM-1 by 42 folds; while Ca^{2+} decreased the affinity by 2 folds.

Since $\alpha_L\beta_2$, $\alpha_M\beta_2$, and $\alpha_X\beta_2$ share overlapping specificity for ICAM-1, they all contribute to the measured adhesion frequency. To determine the relative contributions of $\alpha_L\beta_2$, $\alpha_M\beta_2$, and $\alpha_X\beta_2$ to the binding kinetics of neutrophil adhesion and whether there is cooperation between the three integrins, blocking mAbs against individual β_2 integrins were used separately and in combination during the micropipette experiment. Blocking two of the α subunits allowed to us measure the binding of ICAM-1 to an individual integrin; whereas the unblocked data represented concurrent binding of al three β_2 integrins. The kinetic rates and affinities were separately estimated from the single-species data and multiple-species data. The data indicate that the three β_2 integrins bind ICAM-1 independently rather than cooperatively. $\alpha_L\beta_2$ has the highest affinity for ICAM-1 while $\alpha_X\beta_2$ only contribute to binding when activated.

Results

Site densities of α_L, α_M, and α_X subunits

The site densities of α_L, α_M, and α_X subunits were measured by flow cytometry in the presence of HBSS-, Mg^{2+}/EGTA or Ca^{2+}. It is evident from the fluorescent histograms (Figure 6-1) that the expression of α_L, α_M, and α_X subunits on cell surface did not change when cells were treated with Mg^{2+}/2mM EGTA, or Ca^{2+} and were stable over the period of study. The same conditions were as used for micropipette experiments. The site densities of the three α subunits were calculated (Table 6-1). α_L has a slightly higher site density than α_M and α_X.

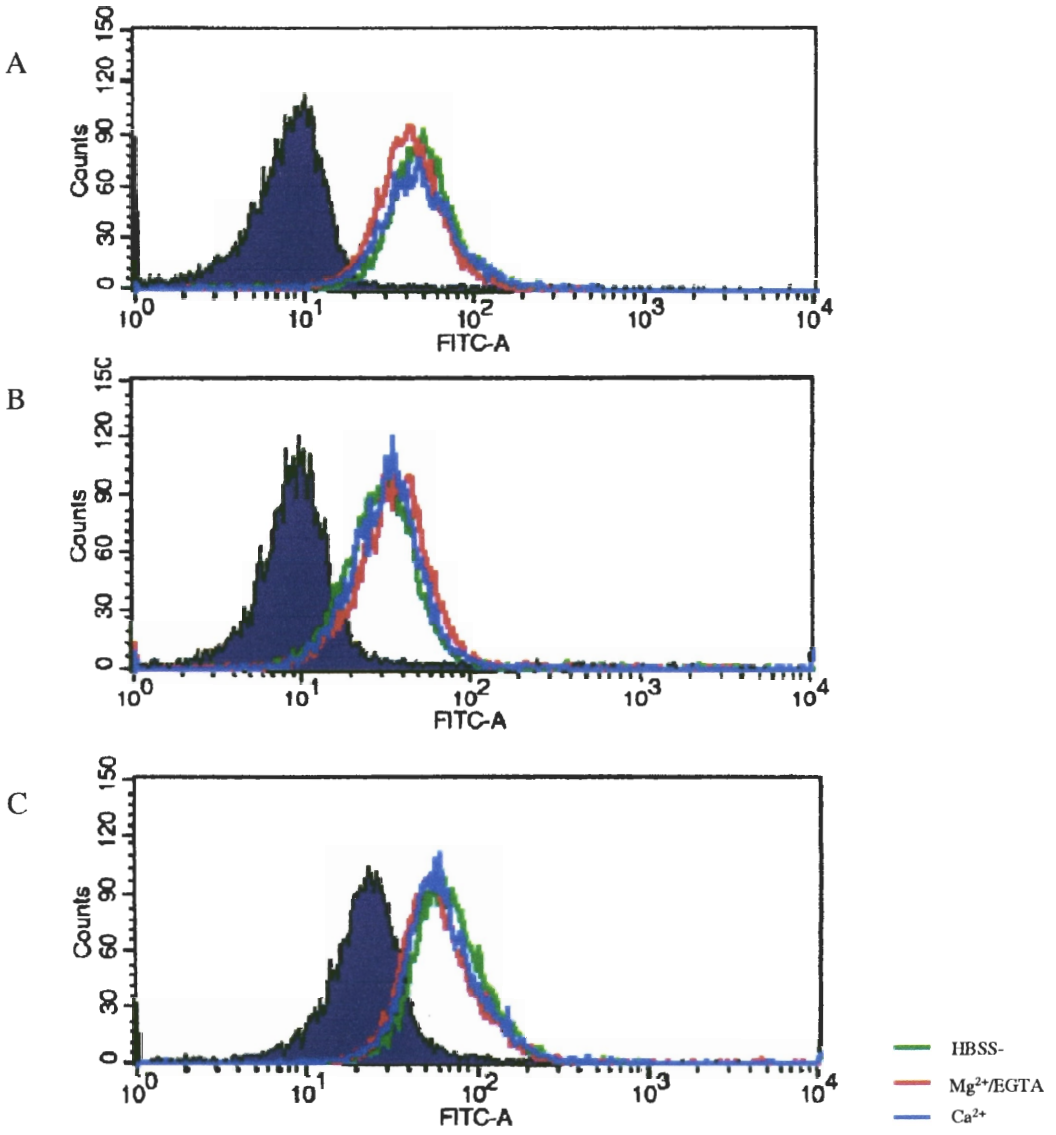

Figure 6-1. Fluorescent histogram of neutrophils. Neutrophils were stained for flow cytometry using (A) mouse anti-human CD11a mouse mAb (DF1524), (B) rat anti-human CD11b (M1/70), or (C) mouse anti-human CD11c (3.9). Isotype matched irrelevant mouse mAb [MOPC-141 for (A) and MOPC-21/P3 for (C)] or rat mAb [KLH/G2b-1-2 for (B)] were used for the background staining (solid peaks). The secondary antibodies were FITC-conjugated goat anti-mouse (or anti-rat) IgG.

Table 6-1. Site densities of α_L, α_M, and α_X subunits on neutrophil. Data were presented as mean ± S.E.M. of the site densities on neutrophil of three donors.

	Site density (sites/μm^2)		
	HBSS-	Mg^{2+}/EGTA	Ca^{2+}
αL	42 (±6)	48 (±7)	47 (±5)
αM	32 (±5)	34 (±8)	31 (±4)
αX	22 (±2)	20 (±3)	24 (±1)

Binding of ICAM-1 to $\alpha_L\beta_2$, $\alpha_M\beta_2$, and $\alpha_X\beta_2$ at different conformational states

The overall binding kinetics of ICAM-1 for neutrophil integrins was measured in HBSS- with or without Mg^{2+}/EGTA and/or Ca^{2+}. Under these conditions, $\alpha_L\beta_2$, $\alpha_M\beta_2$, and $\alpha_X\beta_2$ were treated as a surrogate single species. By fitting the single-species model (Equation 2-4) to the data, we extracted the weighted sum of effective affinities and the reverse rates, or apparent effective affinities and apparent reverse rates. The apparent effective affinity of Mg^{2+} treated neutrophil was ~40 folds higher than that treated with Ca^{2+} (Table 6-2). The apparent reverse rates of HBSS- and Mg^{2+} treated neutrophils were similar, which was about half of the Ca^{2+} treated neutrophils.

Table 6-2. Summary of apparent kinetic rates of ICAM-1 for neutrophil β_2 integrins.

	$A_cK_a^*$ (μm^4)	k_r^* (s^{-1})
HBSS-	1.94(±0.57) E-5	0.27(±0.03)
Mg^{2+}/EGTA	3.11(±0.19) E-4	0.36(±0.07)
Ca^{2+}	7.44(±0.01) E-6	0.85(±0.05)

$A_cK_a^* = A_c\sum_{i=1}^{3} r_iK_{ai}$ ($r_i=m_{ri}/(m_{r1}+ m_{r2+} m_{r3})$, $i=1,2,3$); $k_r^* = \dfrac{\sum_{i=1}^{3} m_{ri}K_{ai}k_{ri}}{\sum_{i=1}^{3} m_{ri}K_{ai}}$

Independent binding of $\alpha_L\beta_2$, $\alpha_M\beta_2$, and $\alpha_X\beta_2$

Using blocking antibodies, binding of individual β_2 integrins to ICAM-1 was assessed. In the presence of Mg^{2+}/EGTA, three β_2 integrins had different binding kinetics to ICAM-1 (Figure 6-3). The kinetic rates and effective affinities were separately estimated from the single-species data (where two out of three α subunits were blocked) and multiple-species data (where all three β_2 integrins could bind concurrently). For the multiple-species data estimation, concurrent binding model (Equation 2-5) was used. In this case, I=3. Using the concurrent binding model involves the simultaneous determination of six parameters. Estimated kinetics rates are listed in Table 6-3.

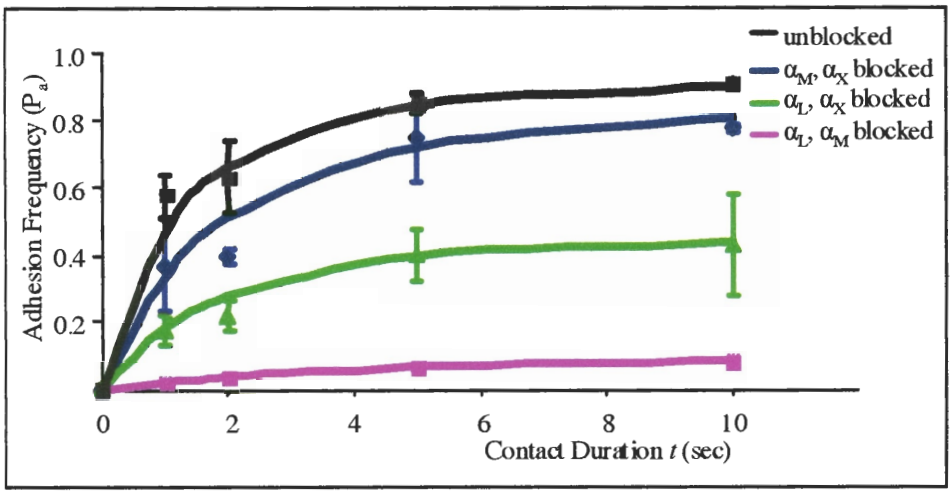

Figure 6-2. Binding curves of ICAM-1 interacting with $\alpha_L\beta_2$, $\alpha_M\beta_2$, or $\alpha_X\beta_2$ individually or concurrently in the presence of Mg^{2+}/EGTA. Each point represents mean adhesion frequency ± S.E.M. of 3 pairs of cells with 100 contacts each. Curves indicate best-fit solutions of the adhesion frequency binding model of Chesla *et al.* (1998) to the blocked data or of the concurrent binding model of Zhu & Williams (2000) to the unblocked data.

Table 6-3. The kinetic parameters extracted from two models for three neutrophil β_2 integrins measured in the presence of Mg^{2+}/EGTA.

	Single-species Model		Concurrent Model	
	AcKa (μm^4)	k_r (s^{-1})	*AcKa* (μm^4)	k_r (s^{-1})
$\alpha_L\beta_2$	1.23(±0.12) E-4	0.25(±0.04)	1.23(±0.22) E-4	0.29(±0.05)
$\alpha_M\beta_2$	4.17(±0.56) E-5	0.30(±0.08)	4.64(±0.60) E-5	0.36(±0.08)
$\alpha_X\beta_2$	1.49(±0.37) E-5	0.25(±0.13)	1.68(±0.05) E-5	0.27(±0.06)

Discussion

The binding kinetics of three neutrophil β_2 integrins to ICAM-1 was measured. By fitting the single-species model to the unblocked data, the effective binding affinity returned parameters are the weighted sum of effective affinity and reverse rate for ICAM-1. Neutrophil β_2 integrins showed quite different 2D kinetics and regulation from the isolated α_L I domains and intact $\alpha_L\beta_2$ on K562 cells. The apparent binding affinities of β_2 integrins on resting neutrophils, i.e. measured in HBSS- or Ca^{2+}, were 2 folds higher than respective values of K562 cell $\alpha_L\beta_2$ measured in HBSS- or Ca^{2+}. Treated with Mg^{2+} resulted in a 335-fold increase in binding affinity of K562 WT $\alpha_L\beta_2$ for ICAM-1. By contrast, Mg^{2+} was only able to increase the apparent effective affinity of neutrophil β_2 integrins by 42 folds and the binding affinity was an order of magnitude lower than that of the activated $\alpha_L\beta_2$ and locked open I domain. Therefore, the binding of inactive neutrophil β_2 integrins with or without Ca^{2+} were higher than inactive $\alpha_L\beta_2$ and α_L I domain on K562 cell; whereas those of the active neutrophil β_2 integrin (treated with Mg^{2+}) were lower than the K562 $\alpha_L\beta_2$. One possible explanation is that the cellular environment of neutrophil and K562 cells are different. They have different cell size, cell membrane topology, cell surface molecules, and intracellular signaling system. For example, β_2 integrins are generally excluded from microvilli in most leukocytes (Williams *et al.,* 2001); while a recent study showed that about 30% of LFA-1 is located on microvilli in transfected K562 cells (Abitorabi *et al.,* 1997). It is reported that cellular environment may alter the kinetics of bond formation under flow (Von-Andrian *et al.*, 1995; Abitorabi *et al.,* 1997). Moreover, divalent cations may not have the same effects

to the three neutrophil β_2 integrins. For example, Ca^{2+} has been shown to inhibit $\alpha_L\beta_2$, but not $\alpha_M\beta_2$, mediated adhesion to ligands (Dransfield *et al.,* 1992; Jackson *et al.,* 1994).

By using blocking antibodies, we also measured the binding kinetics of individual β_2 integrins in the presence of Mg^{2+}/EGTA. It is demonstrated that at low shear, $\alpha_L\beta_2$ and $\alpha_M\beta_2$ contribute equally to neutrophil adhesion initially, but their relative contributions differ markedly over the time course of chemotactic stimulation (Neelamegham *et al,* 1998). The micropipette experiments were done in condition without chemotactic stimulation and the data showed that $\alpha_L\beta_2$ has the highest binding affinity, which is consistent with previous result showing that $\alpha_L\beta_2$ has a more dominant role than $\alpha_M\beta_2$ in neutrophil adhesion (Ding *et al.,* 1999). Our data also suggested that the three β_2 integrins bind to ICAM-1 independently without positive or negative cooperation. That is, the binding of one integrin does not affect the binding of another to ICAM-1. Our result is valid when there is no depletion of ligand and thus integrins do not compete for ligand. Because the adhesion frequency binding model assumed that the number of bonds having nonvanishing probabilities is much smaller than both the numbers of receptors and ligands in the contact area available for binding; therefore, the formation of a small number of bonds will not significantly deplete the free receptors and ligands.

CHAPTER VII

DISCUSSION AND FUTURE RECOMMENDATIONS

Summary

We measured and compared the 2D binding kinetics of mouse ICAM-1 for the human WT and mutant isolated α_L I domains and WT whole $\alpha_L\beta_2$ on K562 cells as well as for three β_2 integrins on human neutrophils. The regulations of the binding kinetics by divalent cations were also investigated.

Our results clearly show that the conformational change in I domain is very important for regulating ligand binding affinity of β_2 integrins. The binding affinity of locked open I domain is ~8000-fold higher than that of the closed I domain (Table 7-1). By comparison, the 2D reverse-rates of the I domains were similar (Table 7-1).

Table 7-1. Summary of 2D binding kinetics of ICAM-1 for K562 isolated I domains

	A_cK_a (μm^4)	A_ck_f ($\mu m^4 \cdot s^{-1}$)	k_r (s^{-1})
WT	1.31(±0.03) E-6	6.57(±0.16) E-6	0.51(±0.01)
Open	4.05(±0.48) E-3	1.60(±0.49) E-3	0.41(±0.11)
Closed	5.07(±1.04) E-7	3.35(±0.53) E-7	0.71(±0.25)

Locked I domains were not regulatable by divalent cations, but the affinity of WT

I domain was increased slightly (< 2 folds) by Mg^{2+} and Mn^{2+}. The differences in binding affinity of the I domains and the lack of divalent cation regulation of the locked I domains were due to the disulfide bonds, as the reduction of disulfide bonds by DTT dramatically decreased the binding affinity of the locked open I domain and slightly increased the affinity of the closed I domain. Moreover, the locked I domains became regulatable by divalent cations after DTT treatment.

The conformational change in I domain requires the presence of other domains of the $\alpha_L\beta_2$ integrin. Mg^{2+} and Mn^{2+} only increased the affinity of WT I domain by < 2 folds; however, they increased the affinity of WT whole $\alpha_L\beta_2$ drastically to the level comparable to that of the locked open I domain (Table 7-2).

Table 7-2. Comparison of 2D binding affinities of isolated I domains and whole $\alpha_L\beta_2$ on K562 measured in different conditions.

	A_cK_a (μm^4)
WT I domain HBSS-	1.35(±0.09) E-6
WT I domain Mg^{2+}/EGTA	2.27(±0.18) E-6
WT I domain Mn^{2+}	2.42(±0.19) E-6
Open I domain HBSS-	3.11(±0.36) E-3
WT $\alpha_L\beta_2$ HBSS-	6.18(±0.02) E-6
WT $\alpha_L\beta_2$ Mg^{2+}/EGTA	2.07(±0.07) E-3
WT $\alpha_L\beta_2$ Mn^{2+}	7.04(±1.22) E-3

We also measured the 2D binding kinetics of ICAM-1 for $\alpha_L\beta_2$, $\alpha_M\beta_2$, and $\alpha_X\beta_2$ on human neutrophils. Without blocking, Mg^{2+} increased the apparent effective binding affinity of ICAM-1 for the three β_2 integrins by ~ 40 folds and this apparent effective affinity is 10 folds lower compared to the locked open I domain and activated whole $\alpha_L\beta_2$ on K562 cells (Table 7-3). When activated by Mg^{2+}, $\alpha_L\beta_2$, $\alpha_M\beta_2$, and $\alpha_X\beta_2$ bind to ICAM-1 independently and $\alpha_L\beta_2$ has the highest binding affinity (Table 7-3).

Table 7-3. Summary of 2D binding kinetics of ICAM-1 for the three β_2 integrins on neutrophils.

	$A_cK_a^*$ (μm^4)	k_r^* (s^{-1})
Three β_2 integrins HBSS-	1.95(±0.29) E-5	0.27(±0.05)
Three β_2 integrins Mg^{2+}/EGTA	3.11(±0.57) E-4	0.36(±0.08)
Three β_2 integrins Ca^{2+}	7.44(±0.49) E-6	0.85(±0.38)
	A_cK_a (μm^4)	k_r (s^{-1})
$\alpha_L\beta_2$ Mg^{2+}/EGTA	1.23(±0.12) E-4	0.25(±0.04)
$\alpha_M\beta_2$ Mg^{2+}/EGTA	4.17(±0.56) E-5	0.30(±0.08)
$\alpha_X\beta_2$ Mg^{2+}/EGTA	1.49(±0.37) E-5	0.25(±0.13)

$$A_cK_a^* = A_c\sum_{i=1}^{3} r_iK_{ai} \quad (r_i = m_{ri}/(m_{r1}+m_{r2}+m_{r3}),\ i=1,2,3); \quad k_r^* = \frac{\sum_{i=1}^{3} m_{ri}K_{ai}k_{ri}}{\sum_{i=1}^{3} m_{ri}K_{ai}}$$

2D vs. 3D binding kinetics

The binding kinetics of soluble ICAM-1 to purified isolated I domains as well as whole $\alpha_L\beta_2$ were measured in SPR (Table 7-4) by Shimaoka *et al* (2001) and Labadia *et*

al (1998).

Table 7-4. The kinetic rates and dissociation constants for ICAM-1 to the WT, open and closed αL I domains and the intact $\alpha_L\beta_2$.

Immo. Ligand	Analyte	k_f ($M^{-1}s^{-1}$)	k_r (s^{-1})	K_d (μM)
sICAM-1	WT I domain	2950±400	4.95±0.85	1670±100
sICAM-1	closed I domain	2110±400	2.84±0.27	1760±70
sICAM-1	open I domain	139000±8000	0.0257±0.0015	0.185±0.012
open I domain	sICAM-1	107000±3000	0.0275±0.0028	0.258±0.024
$\alpha_L\beta_2$	sICAM-1	224000±69000	0.0298±0.0069	0.133±0.041

Binding kinetics measured by SPR. Data were from Shimaoka *et al.* (2001), except for that of $\alpha_L\beta_2$, which was from Labadia *et al.* (1998)

These 3D binding affinity data showed that locked open I domain has a 9000-fold higher binding affinity compared to the WT and locked closed I domain, which are in agreement with the trend and extent of change of the 2D binding affinity data measured by our micropipette experiments. By contrast, the difference in the reverse-rates of the locked open and locked closed I domains was 100-fold from the SPR experiment, but only <2-fold from our micropipette experiment. These comparisons are interesting because it has often assumed that the reverse-rates obtained by 3D and 2D measurements should agree because they have the same unit, s^{-1}. By comparison, it is still not known how to convert the binding affinities obtained from 2D and 3D measurements, which

have different dimensions (Dustin *et al.*, 2001). The small differences in the measured reverse-rates raised a question of whether the micropipette assay is capable of detecting large differences in reverse-rate. To address this question, a positive control experiment could be done by replacing the ICAM-1 by a blocking antibody coated on RBC to interact with locked open I domain expressing K562 cells, because blocking antibodies are known to have very slow off-rates. This experiment could help to confirm that the fast off-rate of the high affinity I domains measured by micropipette is indeed fast rather than an artifact resulted from the insensitivity of the experimental system. Moreover, human ICAM-1 was used in the SPR experiments, but mouse ICAM-1 was used in our system. Although mouse ICAM-1 can bind to human LFA-1 (Johnston *et al.*, 1990), it is not clear whether ICAM-1 molecules from different species bind to human LFA-1 with different kinetics. It would be interesting to measure the 2D binding kinetics of GPI-anchored human ICAM-1 for human isolated I domains and the whole LFA-1. This could determine whether the discrepancy in reverse-rates measured in our study and SPR studies is caused by the difference in ICAM-1 molecules from different species.

Experimental system vs. physiological situation

The micropipette experiment measures the binding kinetics of receptor and ligand when they are bound to cell membrane by manipulating cell-cell adhesion at the single cell level. This allows us not only to observe but also to control a single bond adhesion event. The binding kinetics measured in this system reflects the binding characteristics of receptor and ligand molecules in the force-free condition. In physiological conditions, such as when inflammatory cells attach to endothelium cell layer, the binding events are

not as simple as in the experimental setup. The attachment and detachment are affected by blood stream and other environmental factors, and there might be multiple receptor-ligand interactions occurring simultaneously. Moreover, the binding characteristics of receptors and ligands change over time due to intracellular signaling, which could induce conformational change, coupling to adaptor molecules as well as clustering and oligomerization. Therefore, additional experiments are needed in order to further investigate these more complex phenomena.

I domain conformational change vs. integrin global conformational change

Besides the conformational change in the I domain, the global conformational changes in the whole integrin are also important for increasing binding affinity. In inactive state, the whole integrin bends towards the membrane and makes the binding site in I domain difficult for ligand to access, especially for large ligands (Shimaoka *et al.* 2002). Thus, the switchblade-like change is very important for ligand binding regulation. However, the isolated I domain binding kinetics could not address the importance of the global conformational change. The relative contribution of conformational changes in whole integrin and in I domain could be addressed by using the whole $\alpha_L\beta_2$ with locked open or closed I domain. Whole integrin with locked open I domain still adopts the bent conformation; therefore, the increase in binding affinity of the $\alpha_L\beta_2$ with a locked open I domain compared to the inactive WT $\alpha_L\beta_2$ is contributed by the open I domain conformation. On the other hand, when the $\alpha_L\beta_2$ with a locked closed I domain is treated with reagents that induce the switchblade-like conformational change, such as Mn^{2+}

(Takagi *et al.* 2002) and activating antibodies (Shimaoka *et al.* in press), the increase in binding affinity is due to the global conformational change since the I domain is locked in closed conformation.

Outside-in and inside-out signaling

Integrins signal across the plasma membrane in both directions, i.e., inside-in and outside-in (Hynes, 2002). Divalent cations regulate the activity of integrins by directly or indirectly changing or stabilizing different conformations. The activation of integrins by divalent cations, such as Mg^{2+} or Mn^{2+}, is more likely to resemble the effect of outside-in signaling, that is, the signaling induced by the ligand binding (Arroyo *et al.,* 1992; Leitinger *et al.,* 2000). However, the longest contact duration of receptor and ligand in our micropipette assay was 20 s, which may not be enough for the outside-in signaling to be amplified and affect the function of other molecules. This could be circumvented by using alternative technique allowing longer contact time between receptor and ligand such as fluorescence method. Further work to determine the effects of I domain and whole integrin conformational changes on downstream signaling pathways could be interesting. Many integrin-mediated physiological events are initiated from inside the cell; however, the regulation of integrins by the inside-out signaling is not fully understood. Using cytokines or chemokines that activate cells by inducing inside-out signaling could reveal how these signaling affect the conformational change of integrin extracellular domains.

Neutrophil β_2 integrin binding kinetics

The study of neutrophil β_2 integrin binding kinetics and regulation provided

preliminary data for further investigation. Interestingly, the neutrophil β_2 integrins appeared to have different binding kinetics and regulation compared to both the isolated I domains and intact $\alpha_L\beta_2$ on K562 cells. As we discussed in Chapter VI, one possibility is that different integrins might have different activation patterns. The binding kinetics of individual integrin was only measured when neutrophils were treated with Mg^{2+}. The binding kinetics of individual integrin measured in HBSS- and Ca^{2+} will reveal the difference in regulation of the three β_2 integrins by divalent cations. Furthermore, the conclusion of the independent concurrent binding of three β_2 integrins was drawn based on the binding kinetic rates extracted from the binding curves of three-species and single-species measured in Mg^{2+}. The binding curves of two species with one integrin blocked would give another set of kinetic rates of individual integrins, which could provide more data to strengthen our conclusion. Moreover, we need multi-species binding kinetics when neutrophils are treated with HBSS- or Ca^{2+} to test whether the independent concurrent binding is also valid when the neutrophil β_2 integrins are inactive.

REFERENCES

Abitorabi, M. A., Pachynski, R. K., Ferrando, R. E., Tidswell, M., and Erle, D. J. 1997. Presentation of integrins on leukocyte microvilli: a role for the extracellular domain in determining membrane localization. *J. Cell Biol.* **139**, 563-571.

Alonso, J. L., Essafi, M., Xiong, J-P., Stehle, T., and Arnaout, M. A. 2002. Does the integrin αA domain act as a ligand for its βA domain? *Curr. Biol.* **12**, R340-342.

Arroyo, A. G., Sanchez-Mateos, P., Campanero, M. R., Martin-Padura, I., Dejana, E., and Sanchez-Madrid, F. 1992. Regulation of the VLA integrin-ligand interactions through the beta 1 subunit. *J. Cell. Biol.* **117**, 659-670.

Baldwin, E. T., Sarver, R. W., Bryant, G. L Jr, Curry, K. A., Fairbanks, M. B., Finzel, B. C., Garlick, R. L., Heinrikson, R. L., Horton, N. C., Kelley, L. L., Mildner, A. M., Moon, J. B., Mott, J. E., Mutchler, V. T., Tomich, C. S., Watenpaugh, K. D., and Wiley, V.H. 1998. Cation binding to the integrin CD11b I domain and activation model assessment. *Structure.* **6**, 923-935.

Beglova, N., Blacklow, S. C., Takagi, J., and Springer, T. A. 2002. Cysteine-rich module structure reveals a fulcrum for integrin rearrangement upon activation. *Nat. Struct. Biol.* **9**, 282-287.

Blackford J., Keid, H. W., Pappin, D. J., Bowers, P.S., and Wilkinson, J.M. 1996. A monoclonal antibody, 3/22, to rabbit CD11c which reduces homotypic T cell aggregation: evidence that ICAM-1 is a ligand for CD11c/CD18. *Eur. J. Immunol.* **26**, 525-531.

Carman, C. V., and Springer, T. A. 2003. Regulation of integrin avidity: affinity, valency and recent insights into conformational regulation of integrin structure and function. *Curr. Opin. Cell. Biol.* in press.

Carpén, O., Staunton, D. E., and Springer, T. A. 1992. Association of intercellular adhesion molecule-1 (ICAM-1) with actin-containing cytoskeleton and a-actinin. *J Cell. Biol.* **118**, 1223-1234.

Chesla, S. E., Selvaraj, P., and Zhu, C. 1998. Measuring two-dimensional receptor-ligand binding kinetics by micropipette. *Biophys J.* **75**, 1553-1572.

Crowley, C. A., Curnutte, J. T., Rosin, R. E. Andre-Schwartz, J., Gallin, J. I., Klempner, M., Snyderman, R., Southwick, F. S., Stossel, T. P., and Babior, B. M. 1980. An inherited abnormality of neutrophil adhesion: its genetic transmission and its association with a missing protein. *New Engl J Med.* **302**, 1163-1168.

Danilenko, D. M., Rossitto, P. V., Vander, V. M., Le, T. H., McDonough, S. P., Affolter, V. K , and Moore, P. F. 1995. A novel canine leukointegrin, alpha d beta 2, is expressed by specific macrophage subpopulations in tissue and a minor CD8+ lymphocyte subpopulation in peripheral blood. *J. Immunol.* **155**, 35-44.

Dickeson, S. K., and Santoro, S. A. 1998. Ligand recognition by the I domain-containing integrins. *Cell. Mol. Life. Sci.* **54**, 556-566.

Ding, Z. M., Babensee, J. E., Simon, S. I., Lu, H., Perrard, J. L., Bullard, D.C., Dai, X. Y., Bromley, S. K., Dustin, M. L., Entman, M. L., Smith, C. W., and Ballantyne, C. M. 1999. Relative Contribution of LFA-1 and Mac-1 to Neutrophil Adhesion and Migration. *J Immunol.* **163**, 5029-5038.

Dransfield, I., Cabanas, C., Craig, A., and Hogg, N. 1992. Divalent cation regulation of the function of the leukocyte integrin LFA-1. *J. Cell Biol.* **116,** 219–226.

Du, X., Gu, M., Weisel, J. W., Nagaswami, C., Bennett, J. S., Bowditch, R., Ginsberg, M. H. 1993. Long range propagation of conformational changes in integrin $\alpha_{IIb}\beta_3$.. *J. Biol. Chem.* **268**, 23087-23092.

Dustin, M. L., Rothlein, R., Bhan, A. K., Dinarello, C. A., and Springer, T. A. 1986. Induction by IL 1 and interferon-gamma: tissue distribution, biochemistry, and function of a natural adherence molecule (ICAM-1). *J. Immunol.* **137**, 245-254.

Dustin, M. L., Ferguson, L. M., Chan, P. Y., Springer, T. A., and Golan, D.E.1996. Visualization of CD2 interaction with LFA-3 and determination of the two-dimensional dissociation constant for adhesion receptors in a contact area. *J. Cell. Biol.* **132**, 465-474.

Dustin, M. L., Bromley, S. K., Davis, M. M., and Zhu, C. 2001. Identification of self through two-dimensional chemistry and synapses, *Annu. Rev. Cell Dev. Biol.* **17**, 133-157.

Emsley, J., King, S., Bergelson, J. M., and Liddington, R. C. 1997. Crystal structure of the I domain from integrin a2b1. *J. Biol. Chem.* **272**, 28512-28517.

Emsley, J., Knight, C. G., Farndale, R. W., Barnes, M. J., and Liddington, R. C. 2000. Structural basis of collagen recognition by integrin a2b1. *Cell.* **100**, 47–56.

Evans, E., Berk, D., and Leung, A. 1991. Detachment of agglutinin-bonded red blood cells. I. Forces to rupture molecular-point attachments. *Biophys. J.* **59**, 838–848.

Evans, E., Ritchie, A. K., and Merkel, R. 1995. Sensitive force technique to probe molecular adhesion and structural linkages at biological interfaces. *Biophys. J.* **68**,

2580 –2587.

Griggs, D. W., Schmidt, C. M., and Carron, C. P. 1998. Characteristics of cation binding of the I domains of LFA-1 and MAC-1. *J. Biol. Chem.* **273**, 22113-22119.

Gomes, P., and Andreu, D. 2002. Direct kinetic assay of interaction between small peptide and immobilized antibodies using a surface plasmon resonance biosensor. *J. Immunol. Methods.* **259**, 217-230.

Goodman, T. G., and Bajt, M. L. 1996. Identifying the putative metal ion-dependent adhesion site in the β2 (CD 18) subunit required for αLβ2 and αMβ2 ligand interactions. *J. Biol. Chem.* **271,** 23729–23736.

Humphries, M. J. 2000, Integrin Structure. *Biochem. Soc Trans*. **28**, 311-339.

Hynes, R. O. 2002. Integrins: Bidirectional, Allosteric Signaling Machines. *Cell*. **110,** 673-687.

Jackson, A. M., Alexandroff, A. B., Lappin, M. B., Esuvaranathan, K., James, K., and Chisholm, G. D. 1994. Control of leucocyte function-associated antigen-1-dependent cellular conjugation by divalent cations. *J. Immunol.* **81**, 120-126.

Johnston, S. C., Dustin, M. L., Hibbs, M. L., and Springer, T. A. 1990. On the species specificity of the interaction of LFA-1 with intercellular adhesion molecules. *J. Immunol.* **145**, 1181-1187.

Kallen, J., Welzenbach, K., Ramage, P., Geyl, D., Kriwacki, R., Legge, G., Cottens, S., Weitz-Schmidt, G., and Hommel, U. 1999. Structural basis for LFA-1 inhibition upon lovastatin binding to the CD11a I-domain. *J. Mol. Biol.* **292**, 1–9.

Kamata, T., Tien, K. K., Tarui, T., Puzon-McLaughlin, W., Hogg, N., and Takada, Y. 2002. The role of the CPNKEKEC sequence in the β_2 subuint I domain in regulation of integrin $\alpha_L\beta_2$ (LFA-1). *J. Immunol*. **168**, 2296-2301.

Knorr, R., and Dustin, M. L. 1997. The lymphocyte function-associated antigen 1 I domain is a transient binding module for intercellular adhesion molecule (ICAM) –1 and ICAM-3 in hydrodynamic flow. *J Exp. Med.* **186**, 719-730.

Labadia, M. E., Jeanfavre, D. D., Caviness, G. O., and Morelock, M. M. 1998. Molecular regulation of the interaction between leukocyte function-associated antigen-1 and soluble ICAM-1 by di-valent metal cations. *J. Immunol.***161**, 836–842.

Lawrence, M. B., and Springer, T. A. 1991. Leukocytes roll on a selectin at physiologic flow rates: distinction from and prerequisite for adhesion through integrins. *Cell.* **31**, 859-873.

Lee, J-O., Bankston, L. A., Arnaout, M. A., and Liddingminal, R. C. 1995. Two conformations of the integrin A-domain (I-domain): a pathway for activation? *Structure*. **3**, 1333–1340.

Lee, J-O., Rieu, P., Arnaout, M. A., and Liddington, R. 1995b. Crystal structure of the A domain from the a subunit of integrin CR3 (CD11b/CD18). *Cell*. **80**, 631–638.

Legge, G. B., Kriwacki, R. W., Chung, J., Hommel, U., Ramage, P., Case, D. A., Dyson, H. J., and Wright, P. E. 2000. NMR solution structure of the inserted domain of human leukocyte function associated antigen-1. *J. Mol. Biol.* **295**, 1251–1264.

Leitinger, B., and Hogg, N. 2000. Effects of I domain deletion on the function of the β2 integrin lymphocyte function-associated antigen-1. *Mol. Boil. Cell.* **11**, 677-690.

Leitinger, B., McDowall, A., Stanley, P., and Hogg, N. 2000. The regulation of integrin function by Ca^{2+}. *Biochim. Biophys. Acta.* **1498**, 91-98.

Liddington, R., and Bankston, L. 1998. The integrin I domain: crystal, metals and related artifacts. *Structure*. **6**, 937-938.

Long, M., Zhao, H., and Zhu, C. 2001. Kinetic measurements of cell surface E-selectin/carbohydrate ligand interactions. *Ann Biomed Eng* .**29**, 935-946.

Lu, C., Shimaoka, M., Ferzly, M., Oxvig, C., Takagi, J., and Springer, T. A. 2000. An isolated, surface-expressed I domain of the integrin aLb2 is sufficient for strong adhesive function when locked in the open conformation with a disulfide bond. *Proc. Natl. Acad. Sci. U. S. A.* 98, 2387-2392.

Lu, C. and Springer, T.A. 1997. The α subunit cytoplasmic domain regulates the assembly and adhesiveness of integrin lymphocyte function-associated antigen-1 (LFA-1). *J. Immunol.* **159**, 268-278.

Lum, A. F.H., Green, C. E., Lee, G. R., Staunton, D. E., Simon, S. I. 2002. Dynamic regulation of LFA-1 activation and neutrophil arrest on intercellular adhesion molecule 1 (ICAM-1) in shear flow. *J. Biol. Chem.* **277**, 20660-20670.

Luo BH, Springer TA, Takagi J. 2003. Stabilizing the open conformation of the integrin headpiece with a glycan wedge increases affinity for ligand. *Proc. Natl. Acad. Sci. U. S. A.* **100**, 2403-2408.

Neelamegham, S., Taylor, A. D., Hellums, J. D., Dembo, M., Smith, C. W., and Simon, C. I. 1997. Modeling the reversible kinetics of neutrophil aggregation under hydrodynamic shear. *Biophys. J.* **72**, 1527-1540.

Nolte. M., Pepinsky, R. B., Venyaminov, SYu., Koteliansky, V., Gotwals, P. J., and Karpusas, M. 1999. Crystal structure of the alpha1beta1 integrin I-domain: insights into integrin I-domain function. *FEBS Lett.* **452**, 379-385.

Oxvig, C., Lu, C., and Springer, T. A. 1999. Conformational changes in tertiary structure near the ligand binding site of an integrin I domain. *Proc. Natl. Acad. Sci. U. S. A.* **96**, 2215-20.

Qu, A., and Leahy, D.J. 1995. Crystal structure of the I domain from the CD11a/CD18 (LFA-1, αLβ2) integrin. *Proc. Natl. Acad. Sci. U. S. A.* **92**, 10277–10281.

Qu, A., and Leahy, D. J. 1996. The role of the divalent cation in the structure of the I domain from the CD11a/CD18 integrin. *Structure.* **4**, 931–942.

Salas, A., Shimaoka, M., Chen, S., Carman, C. V., and Springer, T. A. 2002. Transition from rolling to firm adhesion is regulated by the conformation of the I domain of the integrin LFA-1. *J. Biol. Chem.* **277**, 50255-50262.

Shimaoka, M., Lu, C., Palframan, R., Von-Andrian, U. H., Takagi, J., and Springer, T. A. 2001. Reversibly locking a protein fold in an active conformation with a disulfide bond: integrin α_L I domains with high affinity and antagonist activity in vivo. *Proc. Natl. Acad. Sci. U. S. A.* **98**, 6009–6014.

Shimaoka, M., Salas, A., Yang, W., Weitz-Schmidt, G., and Springer, T. A. 2003. Small molecule integrins antagonists that bind to the β2 subunit I-like domain and activate signals in one direction and block them in the other. *Immunity in press.*

Shimaoka, M., Shifman, J. M., Jing, H., Takagi, J., Mayo, S. L., and Springer, T. A. 2000. Computational Design of an Integrin I Domain Stabilized in the Open High Affinity Conformation. *Nat. Struct. Biol.* **7**, 674-678.

Shimaoka, M., Tagaki, J., and Springer, T. A. 2002. Conformational regulation of integrin structure and function. *Annu. Rev. Biophys. Biomol. Struct.* **31**, 485-516.

Shimaoka, M., Xiao, T., Liu, J. H., Yang, Y., Dong, Y., Jun, C. D., McCormack, A., Zhang, R., Joachimiak, A., Takagi, J., Wang, J. H., and Springer, T. A. 2003. Structures of the α_L I domain and its complex with ICAM-1 reveal a shape-shifting pathway for integrin regulation. *Cell.* **112**, 99-111.

Springer, T. A. 1995. Traffic signals on endothelium for lymphocyte recirculation and leukocyte emigration. *Ann. Rev. Physiol.* **57**, 827-872.

Springer, T. A. 1990. Adhesion receptors of the immune system. *Nature.* **346**, 425-433.

Springer, T. A. 1997. Folding of the N-terminal, ligand-binding region of integrin a-subunits into α β-propeller domain. *Proc. Natl. Acad. Sci. U. S. A.* **94**, 65–72.

Takagi, J., Erickson, H. P., and Springer, T. A. 2001. C-terminal opening mimics "inside-out" activation of integrin α5β1. *Nat. Struct. Biol.* **8**, 412-416.

Takagi, J., Petre, B. M., Walz, T., and Springer, T. A. 2002. Global conformational rearrangements in integrin extracellular domains in outside-in and inside-out signaling. *Cell.* **110**, 599-611.

Takagi, J., and Springer, T. A. 2002. Integrin activation and structural reagrangement. *Immunol. rev.* **186**, 141-163.

Von-Andrian, U. H., Hasslen, S. R., Nelson, R. D., Erlandsen, S. L., and Butcher, E. C. 1995. A central role for microvillous receptor presentation in leukocyte adhesion under flow. *Cell.* **82**, 989-899.

Williams, T. E., Nagarajan, S., Selvaraj, P., and Zhu. C. 2001. Quantifying the impact of membrane microtopology on effective two-dimensional affinity. *J. Biol. Chem.* **276**, 13283-13288.

Xiong, J. P., Li, R., Essafi, M., Stehle, T., and Arnaout M. A. 2000. An Isoleucine-based allosteric switch controls affinity and shape shifting in integrin CD11b A-domain. *J. Biol. Chem.* **275**, 38762-38767.

Xiong, J. P., Stehle, T., Diefenbach, B., Zhang, R., Goodman, S., and Arnaout, M.A. 2001. Crystal structure of the extracellular segment of integrin αVβ3. *Science.* **294**, 339-345.

Xiong, J. P., Stehle, T., Zhang, R., Joachimiak, A., Frech, M., Goodman, S. L., and Arnaout, M. A. 2002. Crystal structure of the extracellular segment of integrin $\alpha_V\beta_3$ in complex with an Arg-Gly-Asp ligand. *Science.* **296**, 151-155.

Zhao, H., Zhu, C., Li, X., Dong, X., Zhuang, F., Wang, X., and Stoltz, J. F. 2000. Tetramethylpyrazine inhibits phytohemagglutinin-induced upregulation of ICAM-1 and LFA-1 mediated leukocyte adhesion. *Clin. Hemorheol. Microcirc.* **23**, 145-151.

Zhu, C., and Williams, T. E. 2000. Modeling concurrent binding of multiple molecular species in cell adhesion. *Biophys. J.* **79**, 1850-1857.